

# Adaptive asymptotic solutions of inflationary models in the Hamilton-Jacobi formalism: Application to T-models

---

Elena Medina<sup>a,1</sup> and Gabriel Álvarez<sup>b</sup>

<sup>a</sup>*Departamento de Matemáticas, Facultad de Ciencias, Universidad de Cádiz, 11510 Puerto Real, Cádiz, Spain*

<sup>b</sup>*Departamento de Física Teórica, Facultad de Ciencias Físicas, Universidad Complutense, 28040 Madrid, Spain*

*E-mail:* [elena.medina@uca.es](mailto:elena.medina@uca.es), [galvarez@ucm.es](mailto:galvarez@ucm.es)

ABSTRACT: We develop a method to compute the slow-roll expansion for the Hubble parameter in inflationary models in a flat Friedmann-Lemaître-Robertson-Walker spacetime that is applicable to a wide class of potentials including monomial, polynomial, or rational functions of the inflaton, as well as polynomial or rational functions of the exponential of the inflaton. The method, formulated within the Hamilton-Jacobi formalism, adapts the form of the slow-roll expansion to the analytic form of the inflationary potential, thus allowing a consistent order-by-order computation amenable to Padé summation. Using T-models as an example, we show that Padé summation extends the domain of validity of this adapted slow-roll expansion to the end of inflation. Likewise, Padé summation extends the domain of validity of kinetic-dominance asymptotic expansions of the Hubble parameter into the fast-roll regime, where they can be matched to the aforesaid Padé-summed slow-roll expansions. This matching in turn determines the relation between the expansions for the number  $N$  of e-folds and allows us to compute the total amount of inflation as a function of the initial data or, conversely, to select initial data that correspond to a fixed total amount of inflation. Using the slow-roll stage expansions, we also derive expansions for the corresponding spectral index  $n_s$  accurate to order  $1/N^2$ , and tensor-to-scalar ratio  $r$  accurate to order  $1/N^3$  for these T-models.

---

<sup>1</sup>Corresponding author.

---

## Contents

<b>1</b>	<b>Introduction</b>	<b>1</b>
<b>2</b>	<b>The Hamilton-Jacobi formalism</b>	<b>6</b>
2.1	Scaled magnitudes	6
2.2	The Hamilton-Jacobi formalism	7
2.3	Phase portrait: separatrices, slow-roll and kinetic dominance	8
<b>3</b>	<b>Asymptotic expansions</b>	<b>12</b>
3.1	The Hubble parameter in the SR stage	13
3.2	The number of e-folds in the SR stage	14
3.3	The Hubble parameter in the KD stage	15
3.4	The number of e-folds in the KD stage	16
<b>4</b>	<b>Matching of the SR and KD asymptotic expansions</b>	<b>17</b>
<b>5</b>	<b>Applications</b>	<b>21</b>
5.1	The total amount of inflation as a function of the initial condition	21
5.2	Second-order SR approximation to $n_s$ and $r$ for T-models	23
5.3	Accuracy of the first- and second-order SR approximations	26
<b>6</b>	<b>Conclusions</b>	<b>29</b>
<b>A</b>	<b>Adapted SR expansions</b>	<b>29</b>
<b>B</b>	<b>Padé approximants</b>	<b>31</b>

---

## 1 Introduction

The dynamical equations for single-field inflationary models defined by a potential  $V(\Phi)$  of an inflaton field  $\Phi$  in a spatially flat Friedmann-Lemaître-Robertson-Walker spacetime can be written as

$$\ddot{\Phi} + 3H\dot{\Phi} + V'(\Phi) = 0, \quad (1.1)$$

$$3M_{\text{Pl}}^2 H^2 = \frac{1}{2}\dot{\Phi}^2 + V(\Phi), \quad (1.2)$$

where a prime denotes the derivative of a function with respect to its argument, dots denote derivatives with respect to the cosmic time  $t$ ,  $H$  is the Hubble parameter defined in terms of the scale factor  $a(t)$  as

$$H = \frac{\dot{a}}{a}, \quad (1.3)$$

and  $M_{\text{Pl}}$  is the reduced Planck mass. During inflation, the inflaton  $\Phi$  is a monotonic function of the cosmic time, and the number of e-folds, defined as

$$N(t) = \log \frac{a(t_{\text{end}})}{a(t)}, \quad (1.4)$$

can be written equivalently as

$$N(\Phi) = \log \frac{a(\Phi_{\text{end}})}{a(\Phi)}, \quad (1.5)$$

and is often used as a time coordinate [1–4], where the subindex “end” denotes magnitudes at the end of the inflationary stage, which corresponds to  $N(\Phi_{\text{end}}) = 0$ .

The standard slow-roll (SR) approximation follows from neglecting the kinetic term  $\dot{\Phi}^2/2$  in eq. (1.2) and substituting the resulting approximation

$$H^2 \approx \frac{V(\Phi)}{3M_{\text{Pl}}^2}, \quad (1.6)$$

into the differential equation

$$\frac{dN}{d\Phi} = \frac{1}{2M_{\text{Pl}}^2} \frac{H(\Phi)}{H'(\Phi)}, \quad (1.7)$$

with the said initial condition  $N(\Phi_{\text{end}}) = 0$ . However, increasingly accurate observational data called for a more accurate expansion of which the standard SR approximation (1.6) would be just the leading term. Liddle, Parsons and Barrow [5] developed such an expansion in the form,

$$H(\Phi)^2 = \frac{V(\Phi)}{3M_{\text{Pl}}^2} \left( 1 + \frac{1}{3}\epsilon_{1,V}(\Phi) - \frac{1}{3}\epsilon_{1,V}(\Phi)^2 + \frac{2}{9}\epsilon_{1,V}(\Phi)\epsilon_{2,V}(\Phi) + \dots \right), \quad (1.8)$$

where

$$\epsilon_{1,V}(\Phi) = \frac{M_{\text{Pl}}^2}{2} \left( \frac{V'(\Phi)}{V(\Phi)} \right)^2, \quad (1.9)$$

$$\epsilon_{n,V}(\Phi) = M_{\text{Pl}}^2 \left( \frac{V'(\Phi)^{n-2} V^{(n)}(\Phi)}{V(\Phi)^{n-1}} \right)^{1/(n-1)}, \quad n = 2, 3, \dots \quad (1.10)$$

Equation (1.8) leads to ensuing expansions for the SR parameters  $\epsilon_n$ , of which there are several definitions. We adopt the definitions given in Ref. [6] (which, incidentally, do not agree with the definitions in Ref. [5]),

$$\epsilon_1(\Phi) = 2M_{\text{Pl}}^2 \left( \frac{H'(\Phi)}{H(\Phi)} \right)^2, \quad \epsilon_{n+1}(\Phi) = \frac{d \ln |\epsilon_n(\Phi)|}{dN}, \quad n = 1, 2, \dots \quad (1.11)$$

For example,

$$\epsilon_1(\Phi) = \epsilon_{1,V}(\Phi) - \frac{4}{3}\epsilon_{1,V}(\Phi)^2 + \frac{2}{3}\epsilon_{1,V}(\Phi)\epsilon_{2,V}(\Phi) + \dots, \quad (1.12)$$

and the standard SR approximation (i.e., the leading term of the standard SR expansion) would be to take  $\epsilon_1(\Phi) \approx \epsilon_{1,V}(\Phi)$ . This is the usual approximation used to compute the spectral index  $n_s$  and the tensor-to-scalar ratio  $r$  for a variety of potentials [7].

The present paper is motivated by the observation that although the computation of the standard SR expansion (1.8) to high order using eqs. (1.9) and (1.10) seems straightforward, in practice it is not always so. The order parameter in the standard SR expansion for  $H(\Phi)$  as given by eqs. (1.8)–(1.10) appears to be  $V(\Phi)^{-1/2}$ , but even for the simplest potentials like monomial potentials, this standard expansion does not lead to a systematic order-by-order series that can be directly summed using rational approximants, and for more complicated potentials with concave, exponentially flat plateaus that seem to give results in good agreement with data from the Planck satellite [8, 9] for the ratio of the amplitude of tensor perturbations to the amplitude of scalar perturbations and with the scalar spectral tilt [1, 10, 11], even carrying out the computation at high order is not straightforward.

Therefore, in this paper we develop a method to compute the SR expansion that is applicable to a wide variety of potentials and which, in essence, adapts the form of the SR expansion to the analytic form of the potential  $V(\Phi)$ , thus allowing a consistent and efficient order-by-order computation. The method is formulated within the Hamilton-Jacobi formalism of Salopek and Bond [12], and turns out to be applicable to a wide class of potentials, including monomial, polynomial, or rational functions of the inflaton, as well as to polynomial or rational functions of the exponential of the inflaton, among which we mention cosmological  $\alpha$ -attractors [1, 2, 11, 13–16] and the subclass of T-models [2, 4, 16, 17] corresponding to Kähler superpotentials  $f(Z) = Z^m$ .

The idea to adapt the SR expansions is to find a suitable variable  $F(\Phi)$  that, if used instead of  $V(\Phi)$ , leads to systematic order-by-order computations. Note that if we factor out the leading behavior of  $H(\Phi)$  by defining

$$\mathcal{H}(\Phi) = \sqrt{3}M_{\text{Pl}} \frac{H(\Phi)}{\sqrt{V(\Phi)}}, \quad (1.13)$$

then  $\mathcal{H}(\Phi)$  satisfies [18] (see Ref. [19] for an equivalent equation for  $\log \mathcal{H}$ ),

$$\mathcal{H}'(\Phi) = \frac{1}{M_{\text{Pl}}} \sqrt{\frac{3}{2}} \sqrt{\mathcal{H}(\Phi)^2 - 1} - \mathcal{V}(\Phi)\mathcal{H}(\Phi), \quad (1.14)$$

where

$$\mathcal{V}(\Phi) = \frac{V'(\Phi)}{2V(\Phi)}, \quad (1.15)$$

and whenever this function is of the form

$$\mathcal{V}(\Phi) = \mathcal{Q}(F(\Phi)), \quad (1.16)$$

where  $F(\Phi) \rightarrow \infty$  as  $\Phi \rightarrow \infty$ , and  $\mathcal{Q}$  has an ensuing Taylor expansion in  $1/F(\Phi)$ , then eq. (1.14) has a formal solution in inverse powers of  $F(\Phi)$ . We point out that using these variables  $F(\Phi)$  does not lead to an essentially different SR expansion in the sense that if it were possible to work with the infinitely many terms of the series, both expansions would ultimately be equivalent. However, using  $F(\Phi)$  (i) leads to a systematic expansion in the sense that only the series for  $\mathcal{Q}$  is required, and (ii) the unavoidable truncation to a finite number of terms is done consistently order-by-order in  $1/F(\Phi)$  (i.e., higher-order terms do not contain contributions from lower-order terms), thereby permitting consistent use of

summation methods. We present the method in the main body of the paper by example using T-models (for which there is a wealth of first-order SR results for comparison), and defer to Appendix A the specific choices of  $F(\Phi)$  that adapt the method to the other families of potentials mentioned earlier and the first few terms of the resulting expansions for  $H(\Phi)$ .

T-models, when written in terms of the canonically normalized field  $\Phi$ , are described by potentials of the form

$$V(\Phi) = \Lambda \left( \tanh^2 \left( \frac{\Phi}{M_{\text{Pl}} \sqrt{6\alpha}} \right) \right)^m, \quad (1.17)$$

where  $\Lambda$ ,  $\alpha$  and  $m$  are positive parameters characterizing the particular model. In the SR approximation, the end of inflation is defined by setting

$$\epsilon_1(\Phi_{\text{end}}) \approx \epsilon_{1,V}(\Phi_{\text{end}}) = 1, \quad (1.18)$$

or, explicitly,

$$\sinh \left( \sqrt{\frac{2}{3\alpha}} \frac{\Phi_{\text{end}}}{M_{\text{Pl}}} \right) = \sqrt{\frac{4m^2}{3\alpha}}, \quad (1.19)$$

which leads to (see Ref. [1], Ref. [4] for the particular case  $m = 1$ , or section 3.2 below)

$$N^{(\text{SR})}(\Phi) = \frac{3\alpha}{4m} \left( \cosh \left( \sqrt{\frac{2}{3\alpha}} \frac{\Phi}{M_{\text{Pl}}} \right) - \sqrt{1 + \frac{4m^2}{3\alpha}} \right). \quad (1.20)$$

However, computing the total amount of inflation in this approach would still require the determination of  $\Phi_{\text{in}}$ , the value of the inflaton at the beginning of inflation. Note that in computing the total amount of inflation in this approximation there are two possible sources of error: the first comes from ignoring altogether the kinetic term in the SR stage (i.e., from the fact that eq. (1.20) is just the leading term of a full SR asymptotic expansion), while the second is that  $\Phi_{\text{in}}$  typically lies in the fast roll stage, well beyond the range of applicability not only of the first order SR approximation but even of higher-order SR approximations. We will show that the range of applicability of asymptotic series for the Hubble parameter derived in the kinetic-dominance (KD) stage [19–21], when appropriately summed as discussed below, extends beyond the KD stage not only into the fast-roll stage, but into the beginning of the SR stage. Therefore the KD series can be matched to the appropriately summed SR series, thereby allowing the determination of  $\Phi_{\text{in}}$  as a function of the initial conditions and the comparison of the ensuing total amount of inflation with purely SR results.

Since the determination of  $\Phi_{\text{in}}$  will require us to go into the KD stage, we mention that dynamical systems theory has been used extensively to obtain global results in inflationary cosmology [22] and in particular for these T-models [23–28]. For instance, Alho and Uggla [28] use a Poincaré compactification of the  $(\Phi, \dot{\Phi})$  phase plane which resolves singular points at infinity and therefore is specially suited to identify all possible asymptotic behaviors and all orbits connecting critical points. However, Hamilton-Jacobi methods are better suited to find and match high-order asymptotic solutions of eqs. (1.1) and (1.2) both in the SR stage and in the KD stage. In fact, Liddle, Parsons and Barrow [5] used this kind

of methods to find asymptotic expansions in the SR stage, Handley et. al. [19–21] in the KD stage, and Martínez Alonso et. al. [18, 29, 30] for a variety of potentials in either or both stages. Particularly relevant for the present paper is Ref. [30], in which Medina and Martínez Alonso find asymptotic expansions for the SR and KD stages for a generalized Starobinsky model,

$$V(\Phi) = \Lambda_1 e^{-\sqrt{6}\lambda\Phi/M_{\text{Pl}}} + \Lambda_2 e^{-\sqrt{6}\mu\Phi/M_{\text{Pl}}} + \Lambda_3, \quad (1.21)$$

where all the parameters are positive,  $\lambda > \mu$ , and  $\Lambda_3$  is chosen so that the minimum of the potential is zero. After rescaling  $\varphi = \sqrt{3/2}\Phi/M_{\text{Pl}}$ , typical expansions for this potential in the KD stage (cf. eq. (47) in Ref. [30]), are asymptotic series in  $e^{-\varphi}$  whose coefficients are polynomials in  $e^{-2\lambda\varphi}$  and  $e^{-2\mu\varphi}$ . However, in the case of T-models the asymptotic expansions in the KD stage turn out to be series in  $e^{-\varphi}$  whose coefficients are not polynomials, but *series* in  $e^{-2\varphi/3\sqrt{\alpha}}$ , whose matching to the series in the SR stage has to be done consistently.

The numerical usage of these expansions to obtain high-accuracy results presents the usual challenges of dealing with asymptotic series. For instance, although partial sums of the SR formal series give an excellent accuracy at large  $\Phi$ , they are not accurate enough in a neighborhood of  $\Phi_{\text{end}}$ . A common method to extend the range of applicability of these (truncated) series is to use rational approximants derived from the power series. In fact, in studying the high-order  $\epsilon_{n,V}(\Phi)$  for the quadratic potential, Liddle, Parsons and Barrow [5] use [1/1] rational, multivariable Canterbury approximants to increase the accuracy provided by simple partial sums towards the end of inflation. As summation method for our asymptotic expansions we use Padé approximants [31], both to obtain accurate results towards the end of the inflation and to show the existence of a certain interval on which the appropriately summed SR and KD expansions are both valid, can be matched, and allow the determination of  $\Phi_{\text{in}}$  mentioned in the previous paragraphs.

The layout of the paper is as follows. In section 2 we set up our notation, review the Hamilton-Jacobi formalism, and discuss briefly the relevant features of the region of the T-models phase portrait close to the origin, illustrating in particular the non-inflationary region  $R_1$ , the inflationary region  $R_2$ , and the slow-roll inflationary region  $R_3$ , and showing that solutions with initial conditions on the plateau of the potential eventually enter the SR region. Section 3 is devoted to the derivation of the four asymptotic solutions (Hubble parameter and number of e-folds in the SR and in the KD stages) that we need for our applications. Here we give the specific choice of  $F(\Phi)$  that adapts the SR expansion for T-models. Section 4 is devoted to the matching of the asymptotic expansions for the Hubble parameter and to the determination of the relation between the asymptotic expansions for the number of e-folds. In this section we also compare our results with the first order approximation to the Hubble parameter in the KD stage derived by Chowdhury, Martin, Ringeval and Vennin [3] using the number of e-folds as the independent variable. In section 5 we present two applications of our results: First, we use the method of matched asymptotic expansions to compute the total amount of inflation as a function of the initial data (which, conversely, allows us to select initial data corresponding to a fixed number of e-folds); and second, we use our SR results to compute consistently the expansions of the spectral index

$n_s(N)$  to order  $1/N^2$  and of the tensor-to-scalar ratio  $r(N)$  accurate to order  $1/N^3$  in the SR approximation. More precisely, we show that for T-models,

$$n_s = 1 - \frac{2}{N} - \frac{2 \log N}{3 N^2} + \frac{n_{s,2}(\alpha, m)}{N^2} + O\left(\frac{(\log N)^2}{N^3}\right), \quad (1.22)$$

and

$$r = \frac{12\alpha}{N^2} + 8\alpha \frac{\log N}{N^3} + \frac{r_2(\alpha, m)}{N^3} + O\left(\frac{(\log N)^2}{N^4}\right), \quad (1.23)$$

where  $n_{s,2}(\alpha, m)$  and  $r_2(\alpha, m)$  are rather involved functions (which we compute) of the model parameters. Note in particular the presence of intermediate logarithmic terms between the two the standard SR approximations [2, 10, 16, 32–35] and the corrections of order  $1/N^2$  for  $n_s(N)$  or  $1/N^3$  for  $r(N)$  given, for example, in Refs. [1, 17, 36], where these logarithmic terms are missing. Note that these are purely SR results (without any use of the KD expansions). We also present illustrative numerical comparisons of the accuracy of the first- and adapted second-order (purely) SR approximations as functions of the number of e-folds and of the parameters of the model. After a summary of our results and the aforementioned Appendix A, we include also a brief Appendix B discussing the specific implementation of Padé approximants used in this paper.

## 2 The Hamilton-Jacobi formalism

In this section we review in some detail the Hamilton-Jacobi formalism of inflationary models. Although our formulation is fairly general, from the very beginning we use a T-model as our main example, both because of its physical relevance and because it permits us to show all the details of the method used to adapt the slow-roll expansion to the analytic form of the potential. In Appendix A we show how to perform this process and give the first few terms of the resulting expansions for the families of potentials mentioned earlier.

### 2.1 Scaled magnitudes

Hereafter we will use the reduced inflaton field  $\varphi$  defined by

$$\varphi = \sqrt{\frac{3}{2}} \frac{\Phi}{M_{\text{Pl}}}, \quad (2.1)$$

the reduced Hubble parameter  $h$  defined by

$$h = 3H, \quad (2.2)$$

and the reduced potential  $v(\varphi)$  defined by

$$v(\varphi) = \frac{3}{M_{\text{Pl}}^2} V(\Phi) = A (\tanh^2(\lambda\varphi))^m, \quad (2.3)$$

where

$$A = \frac{3\Lambda}{M_{\text{Pl}}^2}, \quad \lambda = \frac{1}{3\sqrt{\alpha}}. \quad (2.4)$$

(The constant  $A$  could be absorbed by a rescaling of the cosmic time  $t$ , but it is customary not to do so.) In terms of these reduced variables, eqs. (1.1) and (1.2) read

$$\ddot{\varphi} + h\dot{\varphi} + \frac{1}{2}v'(\varphi) = 0, \quad (2.5)$$

and

$$h^2 = \dot{\varphi}^2 + v(\varphi), \quad (2.6)$$

respectively. Finally, and for later reference, we mention a useful consequence of eqs. (2.5) and (2.6): by taking the derivative of eq. (2.6) with respect to cosmic time and eliminating  $\ddot{\varphi}$  between this derivative and eq. (2.5), we find that

$$\dot{h} = -\dot{\varphi}^2. \quad (2.7)$$

## 2.2 The Hamilton-Jacobi formalism

The main goal of the Hamilton-Jacobi formalism is to determine the reduced Hubble parameter  $h$  as a function of the reduced inflaton  $\varphi$ , i.e., to find functions  $h(\varphi)$  in suitable regions of the  $(\varphi, \dot{\varphi})$  phase space. Since this is only possible in regions where  $\dot{\varphi}$  has a constant sign, we first restrict our study to the regions

$$D = \{(\varphi, \dot{\varphi}) : \varphi \geq 0, \dot{\varphi} < 0\}, \quad (2.8)$$

in the  $(\varphi, \dot{\varphi})$  plane, and

$$R = \{(\varphi, h) : \varphi \geq 0, \sqrt{v(\varphi)} < h < +\infty\}, \quad (2.9)$$

in the  $(\varphi, h)$  plane, which are related via the positive square root of eq. (2.6), or, more formally, by the diffeomorphism  $\Gamma : D \mapsto R$ ,

$$\Gamma(\varphi, \dot{\varphi}) = (\varphi, \sqrt{\dot{\varphi}^2 + v(\varphi)}). \quad (2.10)$$

Note that  $R$  will play the role of the phase space in the Hamilton-Jacobi formalism.

Equation (2.7) shows that each part of a solution  $\varphi(t)$  lying on  $D$  satisfies

$$\dot{\varphi} = -h'(\varphi), \quad (2.11)$$

which substituted into eq. (2.6) yields

$$h'(\varphi)^2 = h(\varphi)^2 - v(\varphi). \quad (2.12)$$

Equations (2.11) and (2.12) are referred to as the Hamilton-Jacobi formalism of inflationary models [5, 12, 18–21, 29, 30, 37, 38]. A few comments are in order. First, note that eq. (2.12) allows us to achieve the main goal of the formalism, i.e., to find  $h(\varphi)$ . Second, by integrating eq. (2.11), each solution  $h(\varphi)$  of eq. (2.12) determines a corresponding solution  $\varphi(t)$  in implicit form,

$$t = - \int_{\varphi(0)}^{\varphi(t)} \frac{d\varphi}{h'(\varphi)}. \quad (2.13)$$

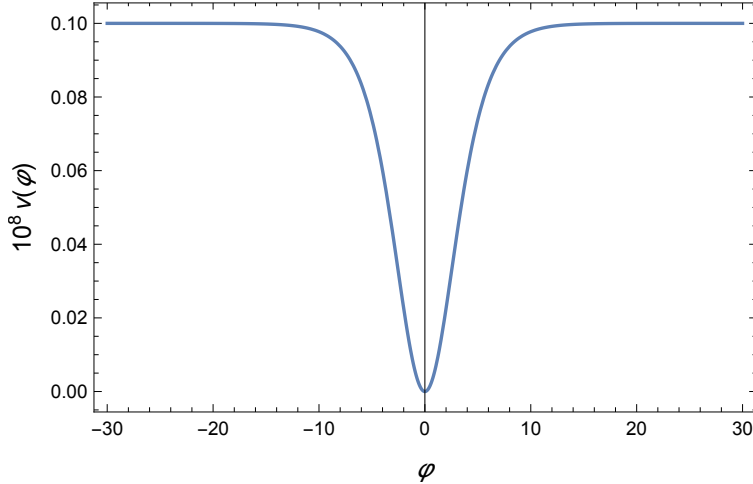


**Figure 1.** Graph of the reduced potential  $v(\varphi) = A (\tanh^2(\lambda\varphi))^m$  for  $A = 10^{-9}$ ,  $\lambda = 1/\sqrt{15}$  and  $m = 1$  (parameters taken from Ref. [2]).

Third, the scale factor can also be determined as a function of  $\varphi$ , since

$$3h'(\varphi)a'(\varphi) + h(\varphi)a(\varphi) = 0, \quad (2.14)$$

and therefore the number of e-folds  $N$  can be also determined as a function of  $\varphi$  via

$$N'(\varphi) = -\frac{a'(\varphi)}{a(\varphi)} = \frac{h(\varphi)}{3h'(\varphi)}. \quad (2.15)$$

Finally, the symmetry

$$(v(\varphi), h(\varphi), \varphi(t)) \rightarrow (v(-\varphi), h(-\varphi), -\varphi(t)) \quad (2.16)$$

of eqs. (2.5), (2.6), (2.7), (2.11) and (2.12) allows us to transfer the results obtained in  $D$  and  $R$  to  $\hat{D} = \{(\varphi, \dot{\varphi}) : \varphi \leq 0, \dot{\varphi} > 0\}$  and  $\hat{R} = \{(\varphi, h) : \varphi \leq 0, \sqrt{v(\varphi)} < h < +\infty\}$ , thereby eliminating our initial restriction.

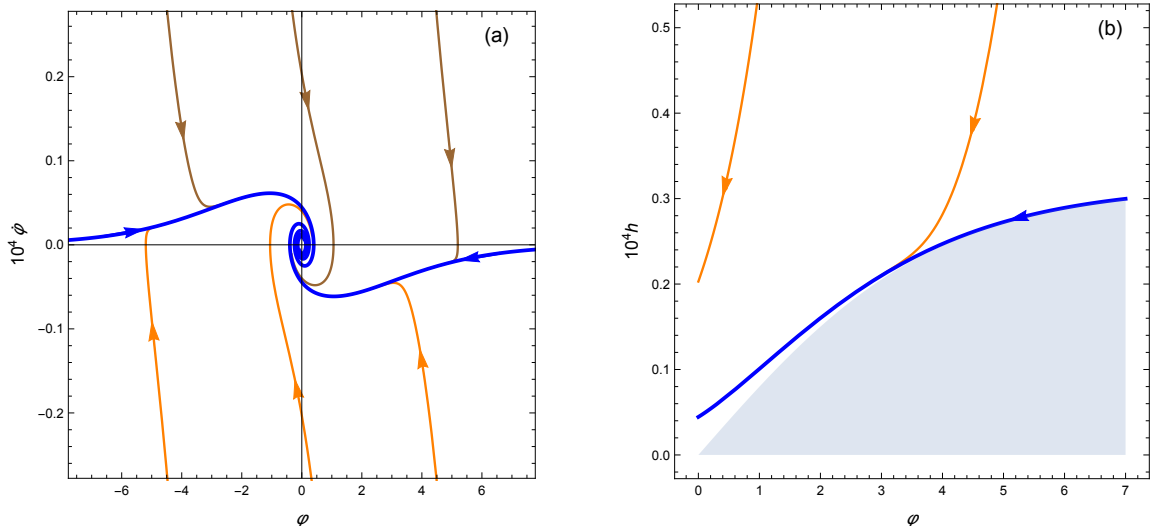
### 2.3 Phase portrait: separatrices, slow-roll and kinetic dominance

Figure 1 shows the graph of the reduced potential eq. (2.3) for one of the examples discussed in Ref. [2], namely  $A = 10^{-9}$ ,  $\lambda = 1/\sqrt{15}$  and  $m = 1$ , where the T-shape that gives name to these potentials and the two concave plateaus are apparent. Note that the minimum value of the potential is  $v_{\min} = v(0) = 0$ .

Figure 2(a) shows the phase portrait for this T-model in the  $(\varphi, \dot{\varphi})$  plane, and figure 2(b) the corresponding phase portrait in the region  $R$  defined by eq. (2.9) of the Hamilton-Jacobi  $(\varphi, h)$  plane, which we now discuss briefly.

In Ref. [18] we proved that, for a certain class of potentials, if

$$\lim_{\varphi \rightarrow \infty} \frac{v'(\varphi)}{2v(\varphi)} = \ell \quad \text{with} \quad 0 \leq \ell < 1, \quad (2.17)$$



**Figure 2.** (a) Phase portrait in the  $(\varphi, \dot{\varphi})$  plane for the potential  $v(\varphi) = A (\tanh^2(\lambda\varphi))^m$  for  $A = 10^{-9}$ ,  $\lambda = 1/\sqrt{15}$  and  $m = 1$ . The two blue trajectories are the separatrices. The region  $D$  defined in eq. (2.8) is the fourth quadrant. (b) Corresponding phase portrait in the region  $R$  defined by eq. (2.9) of the Hamilton-Jacobi  $(\varphi, h)$  plane. The shaded area is the forbidden region where  $h \leq \sqrt{v(\varphi)}$ .

then eq. (2.12) has a unique solution  $h_s(\varphi)$  satisfying

$$h_s(\varphi) \sim \frac{\sqrt{v(\varphi)}}{\sqrt{1-\ell^2}} \quad \text{as } \varphi \rightarrow \infty. \quad (2.18)$$

The T-models given by eq. (2.3) belong to this class of potentials with  $\ell = 0$ . Therefore, eq. (2.12) has a unique solution with asymptotic behavior

$$h_s(\varphi) \sim \sqrt{v(\varphi)} \quad \text{as } \varphi \rightarrow \infty. \quad (2.19)$$

(Incidentally, taking  $h_s(\varphi) \approx \sqrt{v(\varphi)}$  is the standard SR approximation.) This solution, colored blue in figure 2(b), is the boundary in the region  $R$  of the Hamilton-Jacobi phase space between solutions of eq. (2.12) defined for all  $\varphi > 0$  and solutions of eq. (2.12) that leave  $R$  at a certain  $\varphi_m > 0$ . The corresponding (full) trajectory in the  $(\varphi, \dot{\varphi})$  phase plane, also colored blue in figure 2(a), spirals in towards the origin and is part of the boundary between regions filled by trajectories that come from large, positive values of  $\dot{\varphi}$  (colored brown) and large in magnitude, negative values of  $\dot{\varphi}$  (colored orange). The remaining part of the boundary between these trajectories is the symmetric solution. These special solutions are referred to as separatrices, and for wide ranges of initial conditions any solution tends asymptotically to them [5, 22].

In figure 3 we show an enlarged portion of the region  $R$  in the Hamilton-Jacobi  $(\varphi, h)$  plane. From the Hamilton-Jacobi eqs. (2.11) and (2.12) it follows that

$$\ddot{a} = \frac{a}{3} \left( v(\varphi) - \frac{2}{3} h(\varphi)^2 \right), \quad (2.20)$$

and therefore the inflation region  $\ddot{a} > 0$  corresponds to

$$\sqrt{v(\varphi)} < h(\varphi) < \sqrt{\frac{3}{2}v(\varphi)} \quad (2.21)$$

(the lower bound is just eq. (2.9)). As in figure 2, the area shaded in gray in figure 3(a) is the forbidden region  $h \leq \sqrt{v(\varphi)}$ , and the blue curve is the separatrix. The dashed line is the curve  $h(\varphi) = \sqrt{3v(\varphi)/2}$  that separates the non-inflationary region  $R_1$  (white background) from the inflationary region  $R_2$  (light blue shading). Note that not all trajectories enter the inflationary region  $R_2$  (for example, the leftmost trajectory in figure 2(b)), but that all trajectories with initial conditions above the plateau eventually enter  $R_2$ . The gray dots mark the different values  $\varphi_{\text{in}}$  at which these trajectories enter the inflationary region  $R_2$ , while the blue dot marks the *common* value  $\varphi_{\text{end}}$  at which the trajectories leave the inflationary region, after being drawn towards the separatrix. The SR stage is typically defined by,

$$|\epsilon_{1,V}| = \frac{3}{4} \left| \frac{v'(\varphi)}{v(\varphi)} \right|^2 < \varepsilon, \quad |\epsilon_{2,V}| = \frac{3}{2} \left| \frac{v''(\varphi)}{v(\varphi)} \right| < \varepsilon, \quad (2.22)$$

where  $\varepsilon \ll 1$ . Note that these conditions define only an interval  $\varphi \geq \varphi_1$ . To define an SR region  $R_3$  in the  $(\varphi, h)$  plane and following the ideas that lead to the criterion (2.22) we use

$$h(\varphi) \approx \sqrt{v(\varphi)}, \quad \dot{\varphi} \approx -\frac{v'(\varphi)}{2h} \approx -\frac{v'(\varphi)}{2\sqrt{v(\varphi)}}, \quad (2.23)$$

to obtain the improved approximation,

$$h(\varphi) \approx \sqrt{\frac{v'(\varphi)^2}{4v(\varphi)} + v(\varphi)}, \quad (2.24)$$

which allows us to define the ( $\varepsilon$ -dependent, through  $\varphi_1$ ) SR region as

$$R_3 = \left\{ (\varphi, h) : \varphi > \varphi_1 \quad \text{and} \quad \sqrt{v(\varphi)} \leq h \leq \sqrt{\frac{v'(\varphi)^2}{4v(\varphi)} + v(\varphi)} \right\}. \quad (2.25)$$

As an illustration, in figure 3(b) we show a modified phase portrait in which, instead of  $(\varphi, h)$  we plot  $(\varphi, h - \sqrt{v(\varphi)})$  for a value of  $\varepsilon = 1/10$ . Note that the  $R_3$  region extends indefinitely to the right, that the separatrix provides an accurate approximation to the solutions of the T-model in the SR stage, and that  $\varphi_{\text{end}}$  lies outside  $R_3$ .

Let us consider now the behavior of the solutions backwards in the cosmic time  $t$ . Equation (2.7) shows that the reduced Hubble parameter  $h$  is a positive, monotonically decreasing function of  $t$ . Therefore, the reduced Hubble parameter  $h(t)$  increases backwards in time and both  $h(t)$  and  $\varphi(t)$  may develop singularities. In the KD stage, where

$$\dot{\varphi}^2 \gg v(\varphi), \quad (2.26)$$

we may neglect  $v(\varphi)$  in eq. (2.12) and obtain the approximate equation

$$h'(\varphi) \sim \pm h(\varphi), \quad (2.27)$$

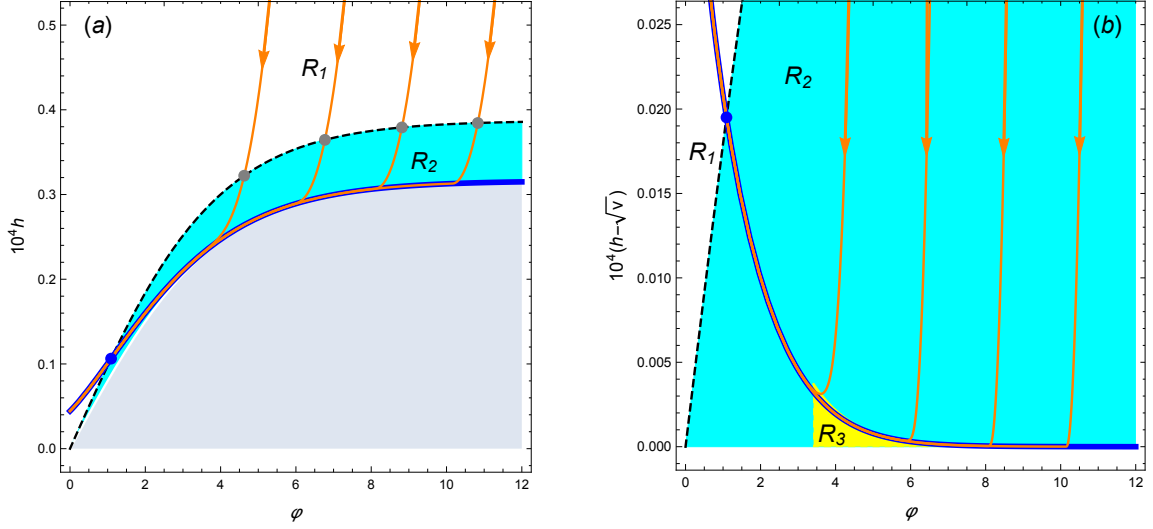


**Figure 3.** (a) Phase portrait in the region  $R$  of the Hamilton-Jacobi  $(\varphi, h)$  plane for the potential  $v(\varphi) = A (\tanh^2(\lambda\varphi))^m$  for  $A = 10^{-9}$ ,  $\lambda = 1/\sqrt{15}$  and  $m = 1$ . As in figure 2, the area shaded in gray is the forbidden region  $h \leq \sqrt{v(\varphi)}$ , and the blue curve is the separatrix. The dashed line is the curve  $h(\varphi) = \sqrt{3v(\varphi)}/2$  that separates the non-inflationary region  $R_1$  (white background) from the inflationary region  $R_2$  (light blue background). The gray dots mark the different values  $\varphi_{\text{in}}$  at which each trajectory enters the inflationary region  $R_2$ , while the blue dot marks the *common* value  $\varphi_{\text{end}}$  at which the trajectories leave the inflationary region, after being drawn towards the separatrix which, although not an attractor in the strict mathematical sense (cf. Ref [18]), effectively works in a similar way. (b) Modified phase portrait  $(\varphi, h - \sqrt{v(\varphi)})$  to show the SR region  $R_3$  corresponding to a value of  $\varepsilon = 1/10$  in eq. (2.25).

which yields two families of approximate solutions

$$h(\varphi) \sim \frac{e^\varphi}{b} \quad \text{as } \varphi \rightarrow \infty, \quad (2.28)$$

and

$$h(\varphi) \sim \frac{e^{-\varphi}}{b} \quad \text{as } \varphi \rightarrow -\infty, \quad (2.29)$$

where  $b$  is a strictly positive but otherwise arbitrary parameter. Incidentally, note that the solution to the initial value problem derived from eqs. (2.11) and (2.28),

$$\dot{\varphi}(t) \approx -\frac{e^{\varphi(t)}}{b}, \quad \varphi(t_0) = \varphi_0, \quad (2.30)$$

is given by

$$\varphi(t) \approx \varphi_0 - \log \left( 1 + \frac{e^{\varphi_0}}{b} (t - t_0) \right), \quad (2.31)$$

and

$$\dot{\varphi}(t) = -\frac{e^{\varphi_0}}{b} \left( 1 + \frac{e^{\varphi_0}}{b} (t - t_0) \right)^{-1}, \quad (2.32)$$

which corresponds to eqs. (4.4a,b) derived by Goldwirth and Piran [39] for their case  $\tilde{\Pi}_0 < 0$ , while the analogous result for their case  $\tilde{\Pi}_0 > 0$ ,

$$\dot{\varphi}(t) = \frac{e^{-\varphi_0}}{b} \left( 1 + \frac{e^{-\varphi_0}}{b} (t - t_0) \right)^{-1}, \quad (2.33)$$

can be derived from our eqs. (2.11) and (2.29).

Again, due to the symmetry eq. (2.16), we can restrict our analysis to solutions with the asymptotic behavior given by eq. (2.28), for which the integral in the right-hand side of Eq (2.13) converges as  $\varphi \rightarrow \infty$ , i.e., these solutions emerge from the KD stage and blow up at a finite time

$$t^* = - \int_{\varphi(0)}^{\infty} \frac{d\varphi}{h'(\varphi)}. \quad (2.34)$$

These singularities, however, lie outside the domain where the KD asymptotic expansions derived in the following section are valid [40].

### 3 Asymptotic expansions

In this section we derive asymptotic expansions for the reduced Hubble parameter  $h(\varphi)$  and the number of e-folds  $N(\varphi)$  both in the SR and in the KD stages. Note that

$$\mathcal{V}(\Phi) = \sqrt{\frac{2}{3\alpha}} \frac{m}{M_{\text{Pl}}} \text{csch} \left( \sqrt{\frac{2}{3\alpha}} \frac{\Phi}{M_{\text{Pl}}} \right), \quad (3.1)$$

and that

$$\text{csch } x = 2 \sum_{n=0}^{\infty} \frac{1}{e^{(2n+1)x}}, \quad \text{as } x \rightarrow \infty. \quad (3.2)$$

Therefore we adapt these expansions to the form of the potential (1.17) by taking the function  $F(\Phi)$  in eq. (1.16) as,

$$F(\Phi) = \exp \left( \sqrt{\frac{2}{3\alpha}} \frac{\Phi}{M_{\text{Pl}}} \right), \quad (3.3)$$

or, in scaled variables,

$$f(\varphi) = e^{2\lambda\varphi}, \quad (3.4)$$

and we take as our new independent variable

$$y = \frac{1}{f(\varphi)} = e^{-2\lambda\varphi}, \quad (3.5)$$

with the corresponding new functions

$$\hat{h}(y) = h(\varphi), \quad (3.6)$$

$$\hat{N}(y) = N(\varphi). \quad (3.7)$$

Substituting eqs. (3.5) and (3.6) into eq. (2.12) with the potential given by eq. (2.3), we find the following equation for  $\hat{h}(y)$ ,

$$4\lambda^2 y^2 \hat{h}'(y)^2 - \hat{h}(y)^2 + A \left( \frac{1-y}{1+y} \right)^{2m} = 0, \quad (3.8)$$

and substituting into eq. (2.15), the following equation for  $\hat{N}(y)$ ,

$$\hat{N}'(y) = \frac{1}{12\lambda^2 y^2} \frac{\hat{h}(y)}{\hat{h}'(y)}. \quad (3.9)$$

### 3.1 The Hubble parameter in the SR stage

As we discussed in section 2.3, the separatrix is an accurate approximation to the solutions in the SR stage, and since the separatrix is uniquely identified by the asymptotic behavior given in eq. (2.19), we look for an asymptotic solution of eq. (3.8) in the form of the leading asymptotic prefactor times a power series in  $y$ ,

$$\hat{h}_{\text{SR}}(y) = \sqrt{A} \left( \frac{1-y}{1+y} \right)^m \left( 1 + 8m^2 \lambda^2 \sum_{n=2}^{\infty} (-1)^n c_n y^n \right). \quad (3.10)$$

By substituting this ansatz into eq. (3.8) we find that  $c_2 = 1$  and that the unknown coefficients  $c_n$  (which depend on  $\lambda$  and  $m$ ) can be computed from the recurrence relation

$$\begin{aligned} c_n = & 8m\lambda^2(n-1)c_{n-1} + 2(1+8m^2\lambda^2)c_{n-2} - 8m\lambda^2(n-3)c_{n-3} - c_{n-4} \\ & - 4m^2\lambda^2 \left( \sum_{j=2}^{n-6} c_j c_{n-4-j} - 2 \sum_{j=2}^{n-4} c_j c_{n-2-j} + \sum_{j=2}^{n-2} c_j c_{n-j} \right) \\ & + 16m^2\lambda^4 \sum_{j=1}^{n-3} [(j+1)c_{j+1} + 2mc_j - (j-1)c_{j-1}] \\ & \times [(n-j-1)c_{n-j-1} + 2mc_{n-j-2} - (n-j-3)c_{n-j-3}], \end{aligned} \quad (3.11)$$

where we have set  $c_n = 0$  for  $n < 2$ . The resulting even and odd coefficients can be written as,

$$c_{2j} = \sum_{k=0}^{j-1} (m\lambda)^{2k} p_{2j}^{(k)}(\lambda^2), \quad (3.12)$$

$$c_{2j+1} = m\lambda^2 \sum_{k=0}^{j-1} (m\lambda)^{2k} p_{2j+1}^{(k)}(\lambda^2), \quad (3.13)$$

respectively, where the  $p_n^{(k)}(\lambda^2)$  are polynomials of degree  $k$  in  $\lambda^2$  which we list in Table 1 up to  $n = 9$ .

$n$	$k$	$p_n^{(k)}(\lambda^2)$
2	0	1
3	0	16
4	0	2
	1	$12 + 448\lambda^2$
5	0	80
	1	$640 + 17408\lambda^2$
6	0	3
	1	$48 + 4096\lambda^2$
	2	$160 + 36352\lambda^2 + 847872\lambda^4$
7	0	224
	1	$4480 + 248832\lambda^2$
	2	$17920 + 2326528\lambda^2 + 49020928\lambda^4$
8	0	4
	1	$120 + 18304\lambda^2$
	2	$960 + 392192\lambda^2 + 17276928\lambda^4$
	3	$2240 + 1714176\lambda^2 + 166674432\lambda^4 + 3255828480\lambda^6$
9	0	480
	1	$17280 + 1612800\lambda^2$
	2	$161280 + 35618816\lambda^2 + 1340866560\lambda^4$
	3	$430080 + 163872768\lambda^2 + 13211009024\lambda^4 + 243139608576\lambda^6$

**Table 1.** Polynomials  $p_n^{(k)}(\lambda^2)$  that give the coefficients  $c_n$  (up to  $n = 9$ ) in the formal expansion of the separatrix  $\hat{h}_{\text{SR}}(y)$  as functions of the parameters  $m$  and  $\lambda$  for the T-models with reduced potentials  $v(\varphi) = A(\tanh^2(\lambda\varphi))^m$ .

### 3.2 The number of e-folds in the SR stage

The corresponding asymptotic expansion for the number of e-folds in the SR stage follows immediately from eq. (3.9),

$$\hat{N}_{\text{SR}}(y) - \hat{N}_{\text{SR},0} = \frac{1}{12\lambda^2} \int \frac{\hat{h}_{\text{SR}}(y) dy}{\hat{h}'_{\text{SR}}(y) y^2}. \quad (3.14)$$

After term by term integration and separation of the leading terms we get an asymptotic expansion which we write in the form

$$\hat{N}_{\text{SR}}(y) - \hat{N}_{\text{SR},0} = \frac{1}{24m\lambda^2} \left( y + \frac{1}{y} \right) - \frac{1}{3} \log y + \sum_{n=1}^{\infty} (-1)^{n+1} \gamma_n y^n. \quad (3.15)$$

Note that there are two terms in  $y$  in this expansion: one in the term between parentheses and one in the formal series. The reason for this choice is that (aside from the dependence of the integration constant) the term in parentheses is the SR approximation eq. (1.20): Indeed, if we integrate eq. (2.15) with the condition  $N(\varphi_{\text{end}}) = 0$ ,

$$N(\varphi) = \frac{1}{3} \int_{\varphi_{\text{end}}}^{\varphi} \frac{h(s)}{h'(s)} ds, \quad (3.16)$$

and use the SR approximation (i.e., the leading term of the SR expansion)  $h(s) \approx \sqrt{v(s)}$ , we find that

$$N_{\text{SR},0}(\varphi) = \frac{2}{3} \int_{\varphi_{\text{end}}}^{\varphi} \frac{v(s)}{v'(s)} ds, \quad (3.17)$$

or, using the reduced form of the potential for T-models (2.3),

$$N_{\text{SR},0}(\varphi) = \frac{1}{12m\lambda^2} \left( \cosh(2\lambda\varphi) - \sqrt{12\lambda^2 m^2 + 1} \right). \quad (3.18)$$

This is eq. (1.20) in reduced variables, and eq. (3.5) leads to

$$\hat{N}_{\text{SR}}(y) - \hat{N}_{\text{SR},0} = \frac{1}{24m\lambda^2} \left( y + \frac{1}{y} \right), \quad (3.19)$$

which is precisely the first term in the right-hand side of eq. (3.15). Incidentally, this result shows that the logarithmic term in eq. (3.15) is a second-order term in the SR expansion.

The coefficients  $\gamma_n$  in eq. (3.15) can be readily calculated from the  $c_2, \dots, c_{n+2}$  during the integration. For example,

$$\gamma_1 = \frac{16}{3} m\lambda^2, \quad (3.20)$$

$$\gamma_2 = \frac{1}{3} + \frac{8}{3} m^2 \lambda^2 + 96 m^2 \lambda^4, \quad (3.21)$$

$$\gamma_3 = \frac{112}{9} m\lambda^2 + \frac{1024}{9} m^3 \lambda^4 + \frac{28672}{9} m^3 \lambda^6, \quad (3.22)$$

but a more efficient method to compute these coefficients is to substitute eqs. (3.10) and (3.15) into eq. (3.9), obtaining directly the relation between the  $\gamma_n$  and the  $c_n$ . Thus, we reproduce eqs. (3.20)–(3.22) and find that for  $n \geq 4$ ,

$$\begin{aligned} \gamma_n = \frac{1}{6n} & \left[ (n+2)c_{n+2} - nc_n + 2mc_{n-1} - 8m\lambda^2((n+1)c_{n+1} + 2mc_n - (n-1)c_{n-1}) \right. \\ & - (1 + 24m\lambda^2\gamma_1)(nc_n + 2mc_{n-1} - (n-2)c_{n-2}) - 48m\lambda^2(n-1)\gamma_{n-1} \\ & \left. - 24m\lambda^2 \sum_{j=3}^{n-1} ((n+2-j)c_{n+2-j} + 2mc_{n+1-j} - (n-j)c_{n-j})(j-1)\gamma_{j-1} \right]. \quad (3.23) \end{aligned}$$

### 3.3 The Hubble parameter in the KD stage

Similarly, to find an asymptotic expansion for the reduced Hubble parameter in the KD stage we have to look for a formal solution of eq. (3.8) with leading asymptotic behavior given by eq. (2.28). However, as we mentioned in the Introduction, and because of this leading asymptotic behavior, this formal solution has to be of the form,

$$\hat{h}_{\text{KD}}(y, b) = \frac{1}{by^{\frac{1}{2\lambda}}} + \sum_{n=1}^{\infty} A^n b^{2n-1} \zeta_n(y) y^{\frac{2n-1}{2\lambda}}, \quad (3.24)$$

where  $\zeta_n(y)$  are in turn formal power series in  $y$ ,

$$\zeta_n(y) = \sum_{p=0}^{\infty} (-1)^p \zeta_{n,p} y^p. \quad (3.25)$$

For the computation of the coefficients  $\zeta_{n,p}$  we assume temporarily that  $\lambda$  is not a rational number, which makes integer powers of  $y$  and of  $y^{\frac{1}{2\lambda}}$  linearly independent, and thus allows independent identification of the corresponding coefficients. A limiting argument shows that our results are still valid for rational values of  $\lambda$ , and a somewhat lengthy computation shows that the coefficients are determined recursively by

$$\zeta_{1,0} = \frac{1}{4}, \quad (3.26)$$

$$\zeta_{1,p} = \frac{1}{4(1+p\lambda)} \sum_{j=1}^p 2^j \binom{2m}{j} \binom{p-1}{j-1}, \quad (p = 1, 2, \dots), \quad (3.27)$$

$$\zeta_{n+1,p} = \frac{1}{n+1+p\lambda} \sum_{j=1}^n \sum_{r=0}^p \left[ \binom{j+r\lambda-\frac{1}{2}}{j} \binom{n-j+(p-r)\lambda+\frac{1}{2}}{j} - \frac{1}{4} \right] \zeta_{j,r} \zeta_{n+1-j,p-r}. \quad (3.28)$$

Since eq. (3.28) for  $p = 0$  takes the form

$$\zeta_{n+1,0} = \frac{1}{n+1} \sum_{j=1}^n \left[ \binom{j-\frac{1}{2}}{j} \binom{n-j+\frac{1}{2}}{j} - \frac{1}{4} \right] \zeta_{j,0} \zeta_{n+1-j,0}, \quad (3.29)$$

by setting  $n = 1$  we find that  $\zeta_{2,0} = 0$ , and by induction that  $\zeta_{n,0} = 0$  for all  $n \geq 2$ . For example, the first three coefficients are,

$$\zeta_1(y) = \frac{1}{4} - \frac{m}{\lambda+1}y + \frac{2m^2}{2\lambda+1}y^2 + \dots, \quad (3.30)$$

$$\zeta_2(y) = -\frac{\lambda m}{4(\lambda+1)(\lambda+2)}y + \frac{\lambda(3\lambda+2)m^2}{2(\lambda+1)^2(2\lambda+1)}y^2 + \dots, \quad (3.31)$$

$$\zeta_3(y) = -\frac{\lambda m}{16(\lambda+2)(\lambda+3)}y + \frac{\lambda(7\lambda^2+16\lambda+6)m^2}{8(\lambda+1)^2(\lambda+2)(2\lambda+3)}y^2 + \dots. \quad (3.32)$$

### 3.4 The number of e-folds in the KD stage

Similarly, asymptotic solutions for the number of e-folds in the KD stage have the form,

$$\hat{N}_{\text{KD}}(y, b) - \hat{N}_{\text{KD},0}(b) = -\frac{\log y}{6\lambda} - \sum_{n=1}^{\infty} A^n b^{2n} \xi_n(y) y^{\frac{n}{\lambda}}, \quad (3.33)$$

where

$$\xi_n(y) = \sum_{p=0}^{\infty} (-1)^p \xi_{n,p} y^p, \quad (3.34)$$

and using eq. (3.9) we find that the coefficients  $\xi_{n,p}$  can be computed recursively from

$$\xi_{1,p} = \frac{1}{3} \zeta_{1,p}, \quad (3.35)$$

and for  $n \geq 2$

$$\xi_{n,p} = \frac{1}{3} \zeta_{n,p} + \frac{1}{n+p\lambda} \sum_{j=1}^{n-1} \sum_{r=0}^p [(j+r\lambda)(2(n-j)+2(p-r)\lambda-1)] \xi_{j,r} \zeta_{n-j,p-r}. \quad (3.36)$$

The first three coefficients are,

$$\xi_1(y) = \frac{1}{12} - \frac{m}{3(\lambda+1)}y + \frac{2m^2}{3(2\lambda+1)}y^2 + \dots, \quad (3.37)$$

$$\xi_2(y) = \frac{1}{96} - \frac{(2\lambda+1)m}{6(\lambda+1)(\lambda+2)}y + \frac{(5\lambda^2+5\lambda+1)m^2}{3(\lambda+1)^2(2\lambda+1)}y^2 + \dots, \quad (3.38)$$

$$\xi_3(y) = \frac{1}{576} - \frac{(9\lambda^2+19\lambda+6)m}{48(\lambda+1)(\lambda+2)(\lambda+3)}y + \frac{(90\lambda^4+313\lambda^3+338\lambda^2+141\lambda+18)m^2}{24(\lambda+1)^2(\lambda+2)(2\lambda+1)(2\lambda+3)}y^2 + \dots. \quad (3.39)$$

#### 4 Matching of the SR and KD asymptotic expansions

In the previous section we have found asymptotic solutions

$$h_{\text{SR}}(\varphi) = \hat{h}_{\text{SR}}(e^{-2\lambda\varphi}), \quad N_{\text{SR}}(\varphi) = \hat{N}_{\text{SR}}(e^{-2\lambda\varphi}), \quad (4.1)$$

and

$$h_{\text{KD}}(\varphi, b) = \hat{h}_{\text{KD}}(e^{-2\lambda\varphi}, b), \quad N_{\text{KD}}(\varphi, b) = \hat{N}_{\text{KD}}(e^{-2\lambda\varphi}, b), \quad (4.2)$$

of eqs. (2.12) and (2.15) valid, in principle, in the SR and KD stages respectively. In this section we discuss how to match these asymptotic solutions to cover the whole inflation region, thereby allowing us to obtain approximate values of relevant magnitudes as functions of the parameter  $b$  in eq. (2.28), or equivalently, as functions of the initial conditions in eq. (2.30),

$$b \approx -\frac{e^{\varphi_0}}{\dot{\varphi}_0} = \frac{e^{\varphi_0}}{\sqrt{h_0^2 - v(\varphi_0)}}, \quad (4.3)$$

which in turn will allow us to find initial conditions that correspond to a previously fixed amount of inflation. This is the layout of the procedure:

1. The  $h_{\text{KD}}(\varphi, b)$  asymptotic expansion, when appropriately Padé-summed, extends its domain of validity beyond the region where eq. (2.26) is satisfied and enters the so-called “fast roll” stage, which allows us to compute the beginning of the inflation interval (2.21) (traveled from right to left in our plots, cf. figure 3) by the condition

$$h_{\text{KD}}(\varphi_{\text{in}}(b), b) = \sqrt{\frac{3}{2}v(\varphi_{\text{in}}(b))}. \quad (4.4)$$

Note that the dependency of  $\varphi_{\text{in}}$  on  $b$  encodes the initial condition.

2. Similarly, the  $h_{\text{SR}}(\varphi)$  asymptotic expansion, when appropriately Padé-summed, extends its domain of validity beyond the SR stage to the value  $\varphi_{\text{end}}$  where inflation ends,

$$h_{\text{SR}}(\varphi_{\text{end}}) = \sqrt{\frac{3}{2}v(\varphi_{\text{end}})}. \quad (4.5)$$

Note that since we have approximated all the solutions in the SR stage by the separatrix, this value  $\varphi_{\text{end}}$  (reached by Padé summation) will be independent of  $b$ .

3. To determine an intermediate value  $\varphi_*(b)$  such that  $h(\varphi)$  is well approximated by  $h_{\text{SR}}(\varphi)$  on  $[\varphi_{\text{end}}, \varphi_*(b)]$ , by  $h_{\text{KD}}(\varphi, b)$  on  $[\varphi_*(b), \varphi_{\text{in}}(b)]$ , and by both on a neighborhood of  $\varphi_*(b)$ , we select  $\varphi_*(b)$  as the first local minimum of  $(h_{\text{KD}}(\varphi, b) - h_{\text{SR}}(\varphi))^2$ , i.e., the local minimum closest to  $\varphi_{\text{in}}(b)$ .
4. Next, to determine the integration constants  $\hat{N}_{\text{SR},0}$  and  $\hat{N}_{\text{KD},0}(b)$  in the asymptotic expansions for  $N$ , we first fix the origin from which we count the amount of inflation by  $N_{\text{SR}}(\varphi_{\text{end}}) = 0$ , i.e.,

$$\hat{N}_{\text{SR}}(e^{-2\lambda\varphi_{\text{end}}}) = 0. \quad (4.6)$$

5. Finally, we determine  $\hat{N}_{\text{KD},0}(b)$  by continuity at  $\varphi_*(b)$ , i.e., by

$$\hat{N}_{\text{SR}}(e^{-2\lambda\varphi_*(b)}) = \hat{N}_{\text{KD}}(e^{-2\lambda\varphi_*(b)}, b). \quad (4.7)$$

Key to this matching procedure is the existence of a neighborhood of  $\varphi_*(b)$  on which the appropriately summed expansions  $h_{\text{SR}}(\varphi)$  and  $h_{\text{KD}}(\varphi, b)$  are both accurate. We consider first the SR asymptotic expansion. The green curve in figure 4 is the result of a numerical integration for the T-model with  $A = 10^{-9}$ ,  $\lambda = 1/\sqrt{15}$  and  $m = 1$  with initial condition  $h(\varphi_0) = 2 \times 10^{-4}$  at  $\varphi_0 = 10$  (outside the range shown in the figure). The shaded region is the inflation region  $R_2$  as defined in eq. (2.21), and the brown, red, and blue curves correspond to the partial sums of the formal series in eq. (3.10) to  $n_{\text{SR}} = 2, 4$  and  $6$  terms, respectively. Figure 4(a) shows that (in part because of the leading behavior as  $\varphi \rightarrow \infty$  built in eq. (3.10)) all these partial sums give excellent approximations at large  $\varphi$ , but the magnification in figure 4(b) shows that partial sums are clearly insufficient to approximate accurately the reduced Hubble parameter in a neighborhood of  $\varphi_{\text{end}} \approx 1.091$ , and, as is typical of partial sums of asymptotic expansions, get progressively worse, despite the fact that the prefactor in eq. (3.10) enforces  $h(0) = 0$ . As we mentioned in the Introduction, faced with an analogous problem (although with fewer terms) for the quadratic potential, Liddle, Parsons and Barrow [5] used [1/1] rational, multivariable Canterbury approximants. However, and in light of the alternating sign apparent in the first terms of eq. (3.10) (for which we do not have a proof), we use Padé  $[n_{\text{SR}}/n_{\text{SR}} + 1]$  approximants to sum the formal series (a brief review of how to compute these approximants is given in Appendix B). At the scale of figure 4, already the [2/3] Padé approximant (not shown) would be superimposed to the numerical integration (green curve). The errors of the Padé approximants at  $\varphi_{\text{end}} \approx 1.091$  (black dot) decrease from 2.14% for  $n_{\text{SR}} = 2$ , to 0.49% for  $n_{\text{SR}} = 4$ , and stabilize at 0.023% for  $n_{\text{SR}} = 12$  and higher approximants, which accounts for the difference between the numerical  $h(\varphi_{\text{end}})$  of our initial value problem and the value of the separatrix at that point to which the asymptotic series  $h_{\text{SR}}(\varphi_{\text{end}})$  is being summed by the Padé approximants.

We consider next the KD asymptotic expansion. Figure 5 shows a neighborhood of  $\varphi_{\text{in}} \approx 8.092$ , where the green curve (barely visible) is the same curve as in figure 4 and the orange curve is the Padé-summed SR asymptotic expansion with  $n_{\text{SR}} = 12$  (as we explained earlier, Padé summation of  $h_{\text{SR}}(\varphi)$  is unnecessary for these values of  $\varphi$  but essential in the neighborhood of  $\varphi_{\text{end}}$ ), and the red and black curves are, respectively, the  $n_{\text{KD}} = 2$  and

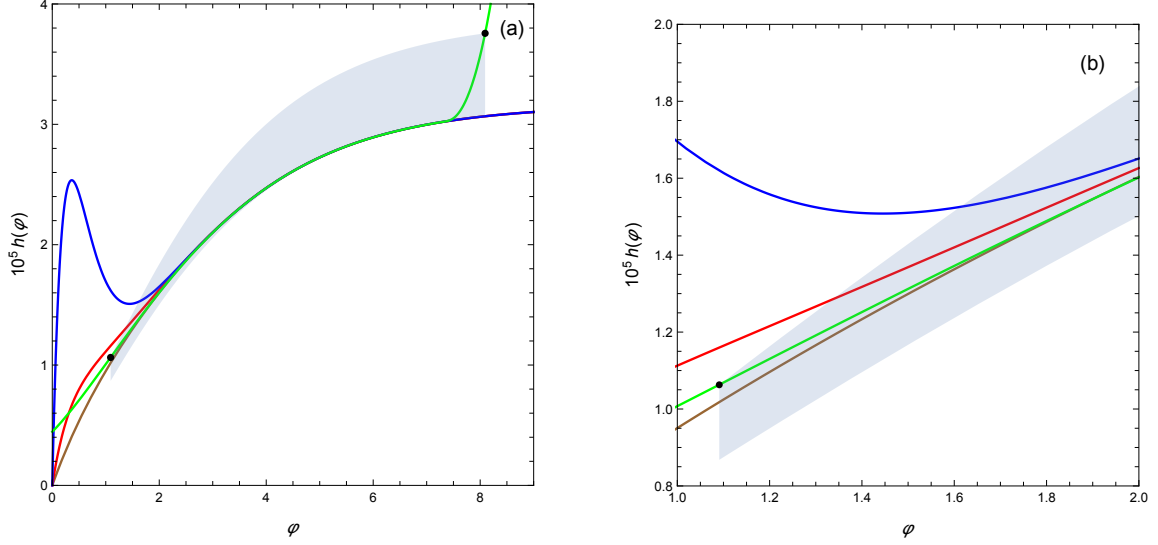


**Figure 4.** Numerical integration (green curve) and partial sums of  $h_{\text{SR}}(\varphi)$  to  $n_{\text{SR}} = 2, 4,$  and  $6$  terms (brown, red and blue curves, respectively) for a T-model with  $A = 10^{-9}$ ,  $\lambda = 1/\sqrt{15}$  and  $m = 1$  with initial condition  $h(\varphi_0) = 2 \times 10^{-4}$  at  $\varphi_0 = 10$  (outside the range of the figure): (a) Inflation region as given by eq. (2.21); (b) Magnification around  $\varphi_{\text{end}} \approx 1.091$ .

$n_{\text{KD}} = 16$  summations of the double series for  $h_{\text{KD}}(\varphi, b)$  with  $b = 1.10817 \times 10^8$ , where, for consistency (and taking into account typical values of  $\lambda$ ), the  $n_{\text{KD}}$  summation is defined by

$$\hat{h}_{\text{KD}}^{[n_{\text{KD}}]}(y, b) = \frac{1}{by^{\frac{1}{2\lambda}}} + \sum_{n=1}^{[2\lambda n_{\text{KD}}]} A^n b^{2n-1} \zeta_{k_n, k_{n+1}}(y) y^{\frac{2n-1}{2\lambda}}, \quad (4.8)$$

where  $[x]$  denotes the greatest integer less than or equal to  $x$ ,

$$k_n = [n_{\text{KD}} - n/(2\lambda)], \quad (4.9)$$

and  $\zeta_{k_n, k_{n+1}}(y)$  denotes the  $[k_n/k_{n+1}]$  Padé approximant to  $\zeta_n(y)$ . The value of  $b$  has been chosen so that the summed  $h_{\text{KD}}(\varphi_0, b) = h(\varphi_0) = h_0$ , and the figure shows that the  $n_{\text{KD}} = 2$  approximation (red curve) does not yet match the SR approximation (orange curve), but the  $n_{\text{KD}} = 16$  (black curve) does match it, and allows us to solve for  $\varphi_*(b)$  as the first local minimum of  $(h_{\text{KD}}(\varphi, b) - h_{\text{SR}}(\varphi))^2$ , which turns out to be  $\varphi_*(b) \approx 7.372$ . Finally, the blue, dashed line represents a noteworthy first order approximation derived by Chowdhury, Martin, Ringeval and Vennin in Ref. [3], which in our notation reads,

$$h(\varphi) \approx \frac{1}{2}(c_+ e^{\varphi - \varphi_0} + c_- e^{-(\varphi - \varphi_0)}), \quad (4.10)$$

where

$$c_{\pm} = h(\varphi_0) \pm \sqrt{h(\varphi_0)^2 - v(\varphi_0)}. \quad (4.11)$$

Figure 5 shows that this approximation is remarkably accurate for a first-order approximation, but is not accurate enough to be matched with the SR approximation.

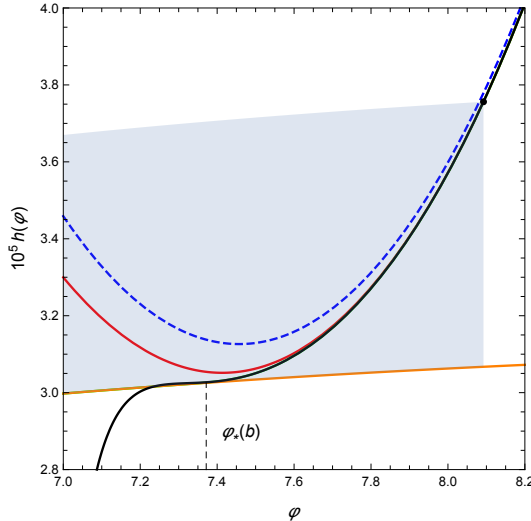


**Figure 5.** Numerical integration of  $h(\varphi)$  (green curve), summation of  $h_{\text{SR}}(\varphi)$  for  $n_{\text{SR}} = 12$ , (orange curve), summations of  $h_{\text{KD}}(\varphi, b)$  for  $n_{\text{KD}} = 2$  (red curve) and  $n_{\text{KD}} = 16$  (black curve), and first-order approximation from Ref. [3] (blue, dashed curve). The vertical line at  $\varphi_*(b) \approx 7.372$  marks the matching point. The numerical (green) curve is barely visible because of the accurate approximations provided by the SR (orange) curve up to  $\varphi_*(b)$  and the KD (black) curve from  $\varphi_*(b)$  onwards.

As we discussed above, the constant  $\hat{N}_{\text{SR},0}$  is a choice of origin determined by eq. (4.6), while matching the asymptotic expansions for the reduced Hubble parameter determines the constant  $\hat{N}_{\text{KD},0}$  in eq. (3.33) via eq. (4.7). In practice we use an expression analogous to eq. (4.8),

$$\hat{N}_{\text{KD}}^{[n_{\text{KD}}]}(y, b) - \hat{N}_{\text{KD},0}(b) = -\frac{\log y}{6\lambda} - \sum_{n=1}^{\lfloor 2\lambda n_{\text{KD}} \rfloor} A^n b^{2n} \xi_{k_n, k_n+1}(y) y^{\frac{n}{\lambda}}, \quad (4.12)$$

but at the risk of being repetitive we stress that the procedure to determine  $\hat{N}_{\text{KD},0}$  is not a matching—the expansions that are matched are the expansions for the reduced Hubble parameter. To illustrate this point, in figure 6 we show the result of the numerical integration for  $N(\varphi)$  (the green curve corresponding to the green curves in figures 4 and 5), the  $n_{\text{SR}} = 16$  summation of  $N_{\text{SR}}(\varphi)$  (the orange curve), and the  $n_{\text{KD}} = 16$  summation of  $N_{\text{KD}}(\varphi, b)$  (the black curve). The magnification in figure 6(b) shows how the matching at  $\varphi_*(b)$  shown in figure 5 induces a crossing between the summations of the expansions for the number of e-folds that mimics the inflection point of the numerical integration. Because of eq. (2.15), the numerical integration for  $N(\varphi)$  is more sensitive to the initial conditions than the numerical integration for  $h(\varphi)$ , but the Padé-summed asymptotic expansion for  $N_{\text{KD}}(\varphi, b)$  gives a remarkably accuracy up to the crossing point.

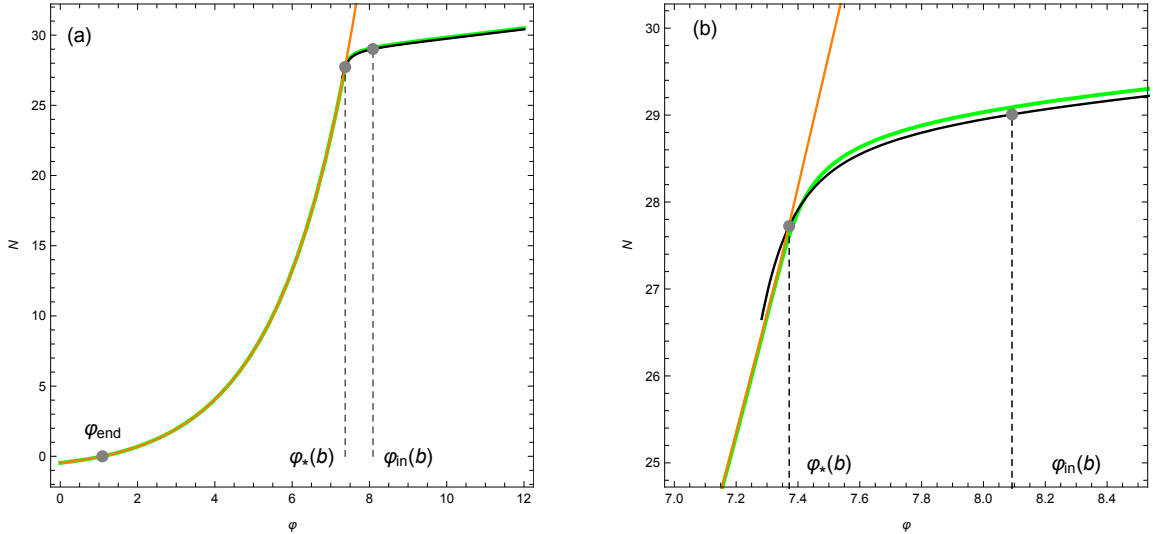


**Figure 6.** Numerical integration for  $N(\varphi)$  (green curve), summation of  $N_{\text{SR}}(\varphi, b)$  for  $n_{\text{SR}} = 16$ , (orange curve), and summation of  $N_{\text{KD}}(\varphi, b)$  for  $n_{\text{KD}} = 16$  (black curve): (a) on the inflation interval  $[\varphi_{\text{end}}, \varphi_{\text{in}}(b)]$ ; (b) magnification of a neighborhood of  $\varphi_*(b)$  showing how the crossing between the summations mimic the inflection point of the numerical integration.

Example	$A$	$m$	$\lambda$
I	$10^{-9}$	1	$1/\sqrt{15}$
II	$10^{-9}$	$7/8$	$1/3$

**Table 2.** Parameters for the T-models used in section 5. The values of  $m$  and  $\lambda$  for Example I and II are taken from Refs. [2], and [16], respectively. The values of  $A$  are derived from typical values of  $\Lambda$ .

## 5 Applications

### 5.1 The total amount of inflation as a function of the initial condition

The approximations to the reduced Hubble parameter  $h(\varphi)$  and to the number of e-folds  $N(\varphi)$  on the whole inflation interval  $[\varphi_{\text{end}}, \varphi_{\text{in}}(b)]$  that the matching procedure discussed in the previous section produces allows us to derive ensuing approximations to several relevant magnitudes as functions of the parameter  $b$  (or, equivalently, of the initial conditions), e.g., the values of the inflaton for which a solution enters and exits the inflation region or the total amount of inflation, or, conversely, to find the initial conditions for a solution to correspond to a previously fixed total amount of inflation.

We illustrate these applications with two examples whose parameters, summarized in Table 2, are chosen according to the following considerations. Our first example has  $m = 1$  and  $\alpha = 5/3$  (or, using eq. (2.4),  $\lambda = 1/\sqrt{15}$ ) [2]. The corresponding values of  $\Lambda$  found in the literature range from  $\Lambda = \alpha 10^{-10} M_{\text{Pl}}^2$  [2, 16] to  $\Lambda = 10^{-8} M_{\text{Pl}}^2$  [4]. Using again eq. (2.4), we have taken as a typical value  $A = 10^{-9}$ . This is the potential shown in figure 1, with the corresponding phase portrait shown in figures 2 and 3, and used for illustrating the several steps of the matching procedure in figures 4–6. Our second example, taken from Ref. [16],

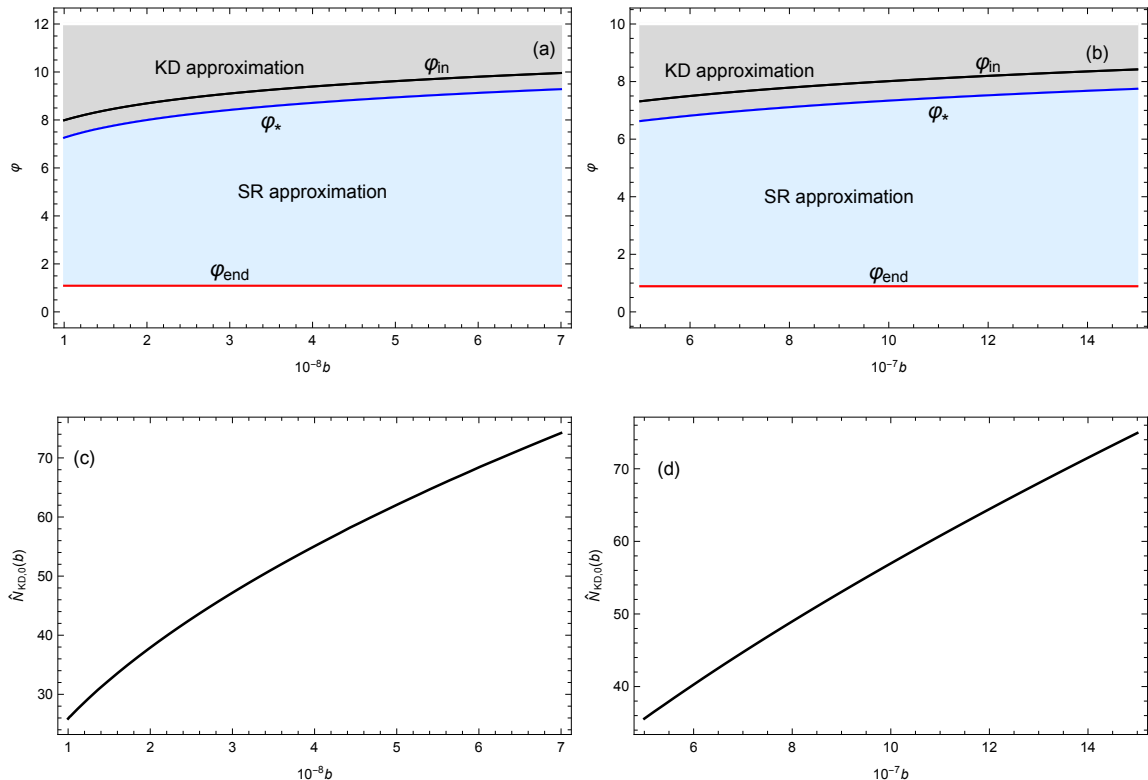


**Figure 7.** Results of the matching of the  $n_{\text{SR}} = 16$  and  $n_{\text{KD}} = 16$  approximants for the T-models of Table 2 as functions of the parameter  $b$ : (a), (b)  $\varphi_{\text{end}}$  (constant, red line),  $\varphi_*(b)$  (blue line) and  $\varphi_{\text{in}}(b)$  (black line) for Example I and Example II respectively; (c), (d)  $\hat{N}_{\text{KD},0}(b)$  for Example I and Example II respectively.

has the noninteger value of  $m = 7/8$ ,  $\alpha = 1$  (i.e.,  $\lambda = 1/3$ ), and again the typical value  $A = 10^{-9}$ . Before proceeding to the applications proper, in Fig 7 we summarize the results of the matching for both examples as a function of the parameter  $b$  for  $n_{\text{SR}} = n_{\text{KD}} = 16$ . The constants  $\hat{N}_{\text{SR},0}$  (determined via eq. (4.6) for Examples I and II are  $-1.69$  and  $-1.31$ , respectively. Figures 7(a) and (b) show the values of  $\varphi_{\text{end}}$  (constant),  $\varphi_*(b)$  and  $\varphi_{\text{in}}(b)$  for Example I and Example II respectively. We recall that the Padé summation provides an SR approximation to the separatrix accurate on  $[\varphi_{\text{end}}, \infty)$ , and a KD approximation for a particular,  $b$ -dependent solution valid on  $[\varphi_*(b), \infty)$ . These intervals are illustrated by the shaded regions in the figure. The values for  $\hat{N}_{\text{KD},0}(b)$  defined in eq. (3.33) and computed according to eq. (4.7) for Examples I and II are shown in figures 7(c) and (d) respectively. The total amount of inflation or number of e-folds during the inflation period is

$$N_T = \log \frac{a(t_{\text{end}})}{a(t_{\text{in}})} = N(\varphi_{\text{in}}) - N(\varphi_{\text{end}}) = N(\varphi_{\text{in}}), \quad (5.1)$$

which we approximate by

$$N_T \approx \hat{N}_{\text{KD}}^{[n_{\text{KD}}]}(e^{-2\lambda\varphi_{\text{in}}(b)}), \quad (5.2)$$

and should be close to  $N_T \approx 60$  [37, 41–43]. Figure 8 shows the result of a calculation with  $n_{\text{SR}} = 16$  and  $n_{\text{KD}} = 16$  for the two examples in Table 2, and Table 3 shows a

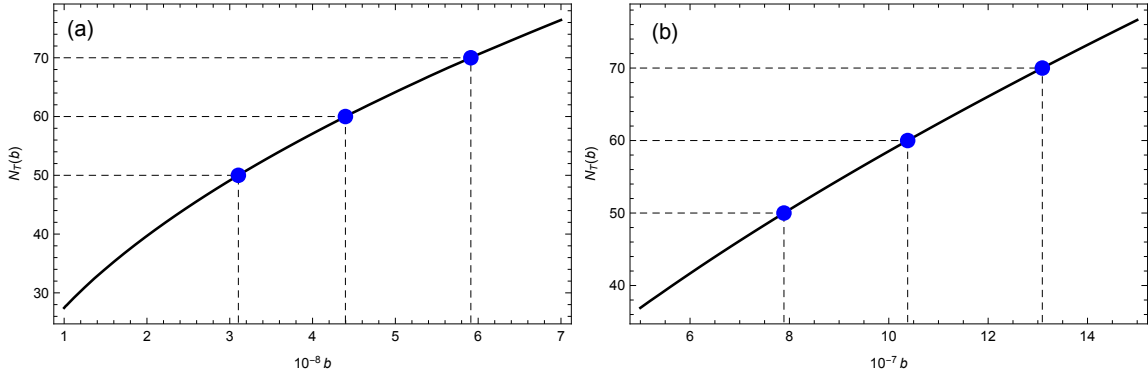


**Figure 8.** Approximate total amount of inflation  $N_T(b)$  as a function of the parameter  $b$  for  $n_{\text{SR}} = 16$  and  $n_{\text{KD}} = 16$ . The dots mark  $N_T = 50, 60$  and  $70$ : (a) Example I in Table 2; (b) Example II in Table 2.

$N_T(b)$	Example I			Example II		
	$b$	$N_T^{(\text{num})}(b)$	$N_{\text{SR}}(\varphi_*(b))$	$b$	$N_T^{(\text{num})}(b)$	$N_{\text{SR}}(\varphi_*(b))$
50	$3.10 \times 10^8$	50.03	48.98	$7.89 \times 10^7$	50.03	48.83
60	$4.40 \times 10^8$	60.00	58.92	$1.04 \times 10^8$	60.06	58.84
70	$5.91 \times 10^8$	70.00	68.93	$1.31 \times 10^8$	70.09	68.85

**Table 3.** Comparison between the total amount of inflation  $N_T(b)$  with  $n_{\text{SR}} = 16$  and  $n_{\text{KD}} = 16$  and the result of a numerical integration from the corresponding initial condition  $b$ .  $N_{\text{SR}}(\varphi_*(b)) = N_{\text{KD}}(\varphi_*(b), b)$  denotes the number of e-folds in the SR stage.

comparison of the results obtained from the asymptotic expansions for  $N_T(b) = 50, 60$  and  $70$  (the marked points on figure 8) with the results of a numerical integration. More concretely, for each value of  $N_T$  we find the corresponding value of  $b$  in figure 8 and perform a numerical integration of eqs. (2.12) and (2.15) with initial conditions at  $\varphi_0 = 10$  given by  $h(\varphi_0) = h_{\text{KD}}(\varphi_0, b)$  and  $N(\varphi_0) = N_{\text{KD}}(\varphi_0, b)$ . In all the cases we have tested, the errors are below 0.5%, i.e., well below one e-fold. Note also that the number of e-folds in the fast-roll stage that the Padé summation of the KD expansion allows us to reach is only of about 1.2, which is consistent with the observation made by Goldwirth and Piran [39] after their eq. (4.13).

## 5.2 Second-order SR approximation to $n_s$ and $r$ for T-models

The spectral index  $n_s$  and the tensor-to-scalar ratio  $r$  for T-models in the first-order SR approximation are given by

$$n_s = 1 - \frac{2}{N}, \quad (5.3)$$

and

$$r = \frac{4}{3\lambda^2 N^2}, \quad (5.4)$$

although the latter equation is often written in terms of  $\alpha$  instead of  $\lambda$  [2, 10, 16, 32–35]. Note in particular that the first-order approximation to  $n_s$  is independent of the parameters

of the model. In this section, and taking advantage of our former SR results, we compute the spectral index  $n_s(N)$  and the tensor-to-scalar ratio  $r(N)$  to second order in the SR approximation or, more precisely, to order  $1/N^2$  and  $1/N^3$  respectively. (We remark that this computation neither uses nor depends in any way of the KD series—the resulting expressions are pure SR results.)

To this aim, we consider the  $O(\epsilon_i^3)$  expressions [6],

$$n_s = 1 - 2\epsilon_1 - \epsilon_2 - 2\epsilon_1^2 - (2C + 3)\epsilon_1\epsilon_2 - C\epsilon_2\epsilon_3, \quad (5.5)$$

and

$$r = 16\epsilon_1 \left[ 1 + C\epsilon_2 + \left( C - \frac{\pi^2}{2} + 5 \right) \epsilon_1\epsilon_2 + \left( \frac{C^2}{2} - \frac{\pi^2}{8} + 1 \right) \epsilon_1^2 + \left( \frac{C^2}{2} - \frac{\pi^2}{24} \right) \epsilon_2\epsilon_3 \right], \quad (5.6)$$

where  $C$  can be written in terms of the Euler-Mascheroni constant  $\gamma$ ,

$$C = \gamma + \log 2 - 2, \quad (5.7)$$

and the slow-roll parameters  $\epsilon_1$ ,  $\epsilon_2$ , and  $\epsilon_3$  can be written as functions of  $N'(\varphi)$  (cf. eq. (2.15)) and its derivatives,

$$\epsilon_1(\varphi) = \frac{1}{3} \frac{1}{N'(\varphi)^2}, \quad (5.8)$$

$$\epsilon_2(\varphi) = -2 \frac{d}{d\varphi} \frac{1}{N'(\varphi)}, \quad (5.9)$$

$$\epsilon_2(\varphi)\epsilon_3(\varphi) = \frac{2}{N'(\varphi)} \frac{d^2}{d\varphi^2} \frac{1}{N'(\varphi)}. \quad (5.10)$$

We will see later that although all the terms in eq. (5.5) are required, only the first two terms in eq. (5.6) need to be considered, i.e.,

$$r = 16\epsilon_1(1 + C\epsilon_2). \quad (5.11)$$

Since all our expansions in this section pertain to the SR stage, hereafter we drop the subindex “SR” but keep the circumflex accent to denote magnitudes in the variable  $y$ . By substituting eq. (3.7) and the second order approximation

$$\hat{N}(y) = \hat{N}_0 + \frac{1}{24m\lambda^2} \left( 1 + \frac{1}{y} \right) - \frac{1}{3} \log y + \frac{16}{3} m\lambda^2 y + O(y^2), \quad (5.12)$$

into eqs. (5.8)–(5.10) we find that,

$$\hat{\epsilon}_1(y) = \frac{48m^2\lambda^2 y^2}{(1-y^2)^2} (1 - 16m\lambda^2 y + O(y^2)), \quad (5.13)$$

$$\hat{\epsilon}_2(y) = \frac{48m\lambda^2 y(1+y^2)}{(1-y^2)^2} (1 - 16m\lambda^2 y + O(y^2)), \quad (5.14)$$

$$\hat{\epsilon}_2(y)\hat{\epsilon}_3(y) = \frac{1152m^2\lambda^4 y^2(1+6y^2+y^4)}{(1-y^2)^4} (1 + O(y)). \quad (5.15)$$

Note that the second order approximation (5.12) differs from the standard SR approximation (3.19) in both the logarithmic term and the first term in the series in eq. (3.15), and that the prefactors in eqs. (5.13)–(5.15) are precisely the first-order SR results.

Then, we need to find the value of  $y_{\text{end}}$  corresponding to the end of the inflationary stage to second order in the SR approximation, i.e., to solve

$$\hat{\epsilon}_1(y_{\text{end}}) = 1 \quad (5.16)$$

to second order. The first order approximation is the suitable solution of the simple bi-quadratic equation

$$\frac{48m^2\lambda^2 y^2}{(1-y^2)^2} = 1, \quad (5.17)$$

namely

$$y_{\text{end},1} = \sqrt{1 + 12m^2\lambda^2} - 2\sqrt{3}m\lambda, \quad (5.18)$$

and the second order correction is obtained by substituting  $y = y_{\text{end},1} + y_{\text{end},2}$  into eq. (5.16) and expanding to first order in  $y_{\text{end},2}$  using eq. (5.13). The full result turns out to be,

$$y_{\text{end}} = (\sqrt{1 + 12m^2\lambda^2} - 2\sqrt{3}m\lambda) \left( 1 + \frac{48m^2\lambda^3}{\sqrt{1 + 12m^2\lambda^2}(6m\lambda + \sqrt{3}\sqrt{1 + 12m^2\lambda^2})} \right). \quad (5.19)$$

Next we need to expand the solution of the equation

$$\hat{N} - \hat{N}_0 = \frac{1}{24m\lambda^2} \left( \frac{1}{y} + y \right) - \frac{1}{3} \log y + \frac{16}{3} m\lambda^2 y, \quad (5.20)$$

for  $y$  as a function of  $\hat{N}$  as  $\hat{N} \rightarrow \infty$  to order  $1/\hat{N}^2$ . In order to do this we consider first the two leading terms in the right-hand side of eq. (5.20),

$$\hat{N} - \hat{N}_0 = \frac{1}{24m\lambda^2 y} - \frac{1}{3} \log y, \quad (5.21)$$

where

$$\hat{N}_0 = -\frac{1}{24m\lambda^2} \left( \frac{1}{y_{\text{end}}} + y_{\text{end}} \right) + \frac{1}{3} \log(y_{\text{end}}) - \frac{16}{3} m\lambda^2 y_{\text{end}}, \quad (5.22)$$

so that  $\hat{N}(y_{\text{end}}) = 0$ . Equation (5.21) can be solved exactly in terms of Lambert's  $W$  function [44],

$$y = \frac{1}{8m\lambda^2 W(e^{3(\hat{N} - \hat{N}_0)}/8m\lambda^2)}, \quad (5.23)$$

which leads to the expansion (cf. again Ref. [44]),

$$y = \frac{1}{24m\lambda^2} \left[ \frac{1}{\hat{N}} + \frac{\log \hat{N}}{3\hat{N}^2} + \frac{3\hat{N}_0 + \log(24m\lambda^2)}{3\hat{N}^2} + O\left(\frac{(\log \hat{N})^2}{\hat{N}^3}\right) \right]. \quad (5.24)$$

To check if this equation is in fact the solution of eq. (5.20) to the order stated we substitute an expansion of the form

$$y = \frac{1}{24m\lambda^2} \left[ \frac{1}{\hat{N}} + \frac{\log \hat{N}}{3\hat{N}^2} + \frac{q}{\hat{N}^2} + \frac{p_2(\log \hat{N})^2}{\hat{N}^3} + \frac{p_1 \log \hat{N}}{\hat{N}^3} + \frac{p_0}{\hat{N}^3} + O\left(\frac{(\log \hat{N})^3}{\hat{N}^4}\right) \right] \quad (5.25)$$

into eq. (5.20), equate to zero in the resulting equation the coefficients of  $\hat{N}^0$  and  $\hat{N}^{-1}(\log \hat{N})^k$ ,  $k = 0, 1, 2$  and find that

$$q = \hat{N}_0 + \frac{1}{3} \log(24m\lambda^2), \quad (5.26)$$

$$p_0 = q^2 - \frac{q}{3} + \frac{2}{9} + \frac{1}{576m^2\lambda^4}, \quad (5.27)$$

$$p_1 = \frac{2}{3}q - \frac{1}{9}, \quad (5.28)$$

$$p_2 = \frac{1}{9}. \quad (5.29)$$

Thus, we confirm that the solution of eq. (5.20) to order  $1/\hat{N}^2$  is indeed given by eq. (5.24). Incidentally, we mention that the first term in which the expansions of the solutions of eqs. (5.20) and (5.21) differ is the term in  $1/\hat{N}^3$ .

Finally, by substituting eq. (5.24) into eqs. (5.13)–(5.15), these in turn into eqs. (5.5) and (5.11), and dropping the circumflex accent of  $N$ , which is now not considered a function but the variable, we arrive at,

$$n_s = 1 - \frac{2}{N} - \frac{2 \log N}{3 N^2} - \frac{2}{N^2} \left( \frac{1}{12\lambda^2} + \hat{N}_0 + \frac{\log(24m\lambda^2) - 2}{3} + C \right) + O\left(\frac{(\log N)^2}{N^3}\right), \quad (5.30)$$

and

$$r = \frac{4}{3\lambda^2 N^2} + \frac{8 \log N}{9\lambda^2 N^3} + \frac{8}{9\lambda^2 N^3} (3\hat{N}_0 + \log(24m\lambda^2) - 1 + 3C) + O\left(\frac{(\log N)^2}{N^4}\right). \quad (5.31)$$

Note the presence of logarithmic terms in the expansions that we mentioned in the Introduction and that are missed in Refs. [1, 17, 36], and the fact that the first correction to the  $n_s$  in eq. (5.3) is still independent of the parameters of the T-model, which appear only in the next term. At the risk of being repetitive, we remark that eqs. (5.30) and (5.31) follow from the standard SR expansion (1.8)—our method of computing this expansion by adapting it to the analytic form of the potential (1.17) makes their derivation both practical and systematic.

### 5.3 Accuracy of the first- and second-order SR approximations

In this section we present some numerical results that illustrate the accuracy of the first- and second-order (purely) SR approximations to the spectral index and tensor to scalar ratio as functions of the number of e-folds and of the parameters of the model. All these results pertain to the T-model given in eq. (2.3) with  $A = 10^{-9}$ .

The first magnitude of interest is the value of the inflaton at the end of inflation  $\varphi_{\text{end}}$ , because its value enters the derivation via eqs. (5.20) and (5.22). In figure 9 we compare the values of  $\varphi_{\text{end}}$  given by the first-order SR approximation eq. (5.18) (red curve), by the second-order SR approximation eq. (5.19) (blue curve), and by a numerical integration (green curve). Figure 9 (a) shows  $\varphi_{\text{end}}$  as a function of the parameter  $m$  for a fixed value  $\lambda = 1/\sqrt{15}$ , and figure 9 (b) shows  $\varphi_{\text{end}}$  as a function of the parameter  $\lambda$  for a fixed value  $m = 1$ . These ranges of  $m$  and  $\lambda$  cover the cases of physical interest, and across all of

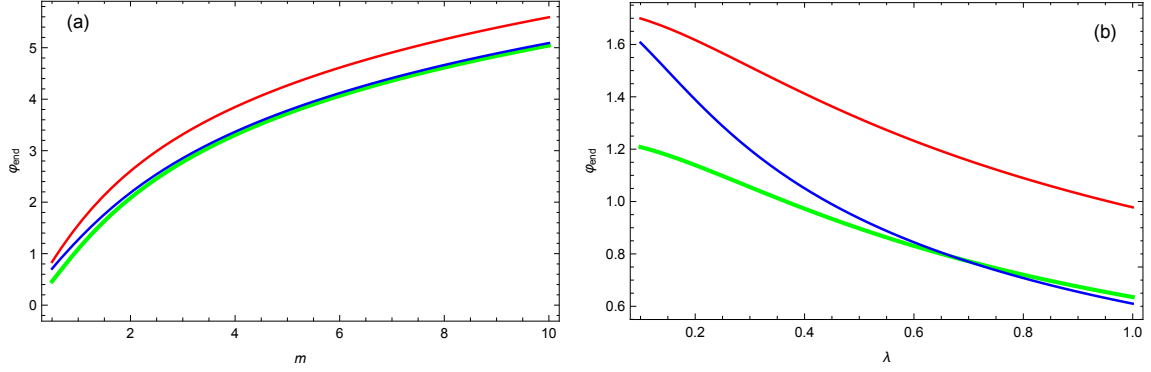


**Figure 9.** End of inflation  $\varphi_{\text{end}}$  for T-models with  $A = 10^{-9}$  and initial condition  $h(\varphi_0) = 4.4 \times 10^{-5}$  at  $\varphi_0 = 10$ . The red curves are the results given by the first-order SR approximation eq. (5.18), the blue curves are the results given by the second-order SR approximation eq. (5.19), and the green curves are the results of numerical integrations: (a) as a function of the parameter  $m$  for a fixed value  $\lambda = 1/\sqrt{15}$ ; (b) as a function of the parameter  $\lambda$  for a fixed value of  $m = 1$ .

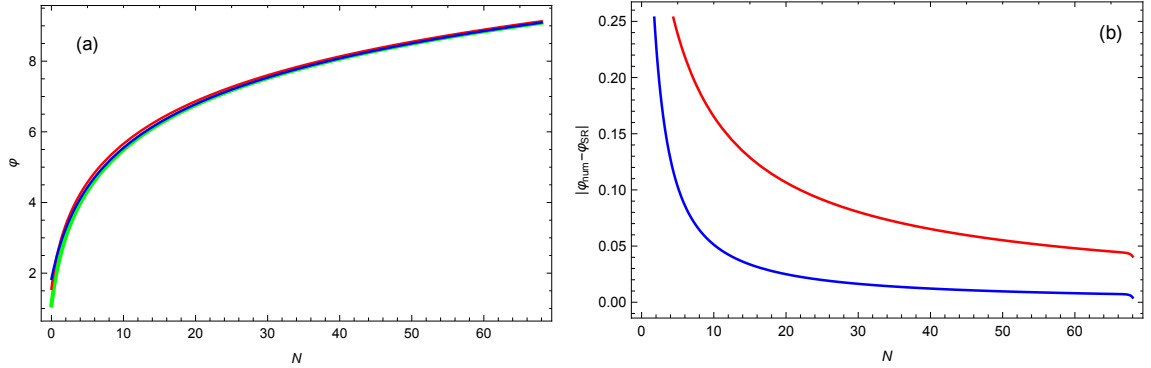


**Figure 10.** (a) Inflation  $\varphi$  as a function of the number of e-folds  $N$  for a T-model with  $A = 10^{-9}$ ,  $m = 1$ ,  $\lambda = 1/\sqrt{15}$  and initial condition  $h(\varphi_0) = 4.4 \times 10^{-5}$  for  $\varphi_0 = 10$  as a function of the number of e-folds  $N$ . The red curve is the first-order SR approximation, the blue curve is the second-order SR approximation, and the green curve is the result of a numerical integration. (b) Absolute values of the differences between the numerical value of the inflaton and its first order (red curve) and second order (blue curve) SR approximations.

them the second-order SR approximation is clearly more accurate than the first-order SR approximation.

In figure 10 (a) we show the value of the inflaton  $\varphi$  as a function of the number of e-folds  $N$  for  $m = 1$  and  $\lambda = 1/\sqrt{15}$ . The red curve is the first-order SR approximation, the blue curve is the second-order SR approximation, and the green curve is the result of a numerical integration. The order of magnitude of  $\varphi$  in this figure does not allow to appreciate the respective accuracies. Therefore, in figure 10 (b) we show for the corresponding differences  $|\varphi_{\text{num}} - \varphi_{\text{SR},1}|$  (red curve) and  $|\varphi_{\text{num}} - \varphi_{\text{SR},2}|$  (blue curve). The second-order SR approximation is clearly more accurate.

Finally, figures 11 and 12 show, respectively, the corresponding results for the spectral

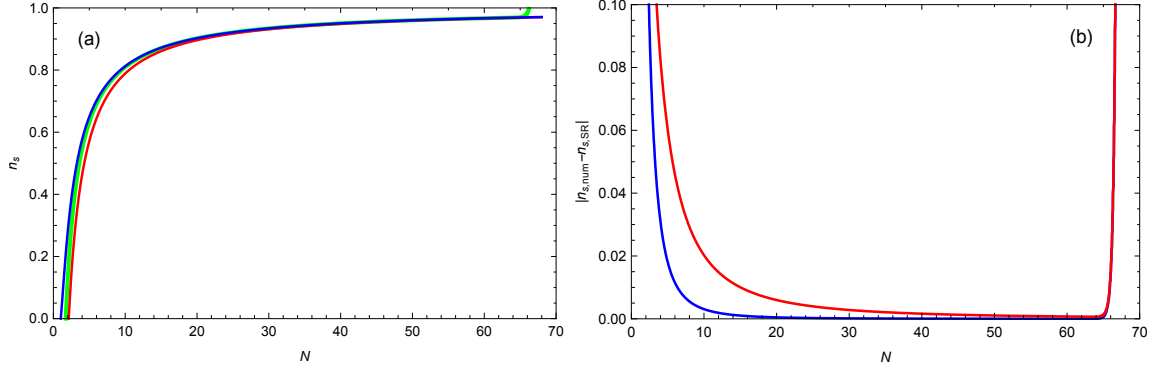


**Figure 11.** (a) Spectral index  $n_s$  for a T-model with  $A = 10^{-9}$ ,  $m = 1$ ,  $\lambda = 1/\sqrt{15}$  and initial condition  $h(\varphi_0) = 4.4 \times 10^{-5}$  for  $\varphi_0 = 10$  as a function of the number of e-folds  $N$ . The red curve is the result given by the first-order SR approximation, the blue curve is the result given by the second-order SR approximation, and the green curve is the result of a numerical integration. (b) Absolute values of the differences between the numerical value of the spectral index and its first order (red curve) and second order (blue curve) SR approximations. In the region beyond  $N = 65$  both curves are superimposed.

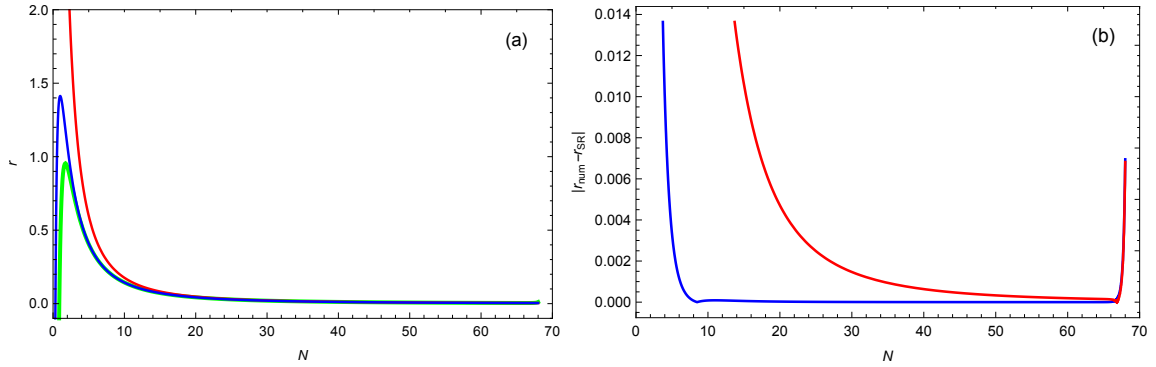


**Figure 12.** (a) Tensor-to-scalar ratio  $r$  for a T-model with  $A = 10^{-9}$ ,  $m = 1$ ,  $\lambda = 1/\sqrt{15}$  and initial condition  $h(\varphi_0) = 4.4 \times 10^{-5}$  for  $\varphi_0 = 10$  as a function of the number of e-folds  $N$ . The red curve is the result given by the first-order SR approximation, the blue curve is the result given by the second-order SR approximation, and the green curve is the result of a numerical integration. (b) Absolute values of the differences between the numerical value of the tensor-to-scalar ratio and its first order (red curve) and second order (blue curve) SR approximations. In the region beyond  $N = 65$  both curves are superimposed.

index  $n_s$  and for the tensor-to-scalar ratio  $r$  for the T-model with  $m = 1$  and  $\lambda = 1/\sqrt{15}$ . Again, the red curves are the first-order SR results, the blue curves are the second-order SR results, and the green curves are the results of numerical integrations. The left panels show the magnitudes, and the right panels the differences between the numerical values and the SR approximations. In the steep arcs beyond  $N = 65$  in both (b) panels the first-order and second-order SR approximations are in fact superimposed. Again, the second-order approximation is more accurate. Both approximations quickly lose accuracy at the beginning of inflation (i.e., beyond  $N = 65$ , well outside the SR region).

## 6 Conclusions

We have shown that the Hamilton-Jacobi formalism, when adapted to the specific inflationary potential, leads to efficient recurrence relations to compute asymptotic expansions for the Hubble parameter in both the SR stage—where, in fact, the expansion corresponds to the separatrix—and in the KD stage—where the expansion depends explicitly on the initial condition. Partial summations of these asymptotic expansions are not accurate enough to describe the complete inflation process, but Padé summations thereof converge quickly and extend their respective domains to allow a successful matching, which in turn determines the relation between the respective asymptotic expansions for the number of e-folds. These SR and KD expansions combined cover the whole inflation period and are much more accurate than well known formulas like eq. (4.10) for the Hubble parameter in the KD stage, or eq. (1.20) for the number of e-folds during the SR stage, and allow us to find the total amount of inflation as a function of the initial data or, conversely, to choose initial data that correspond to a fixed total amount of inflation. The required order of the expansions is determined by the fact that although for a fixed order the accuracy increases with the number of e-folds, to attain a certain accuracy for a fixed number of e-folds may require high-order expansions for the typical values of the T-models parameters  $\lambda$  and  $m$ . In particular, the SR expansions have allowed us to compute consistently expansions for the spectral index  $n_s(N)$  accurate to order  $1/N^2$ , and the tensor-to-scalar  $r(N)$  accurate to order  $1/N^3$ , in which we have found logarithmic terms and the noteworthy fact that the first dependence of  $n_s(N)$  on the model parameters is found precisely in the term proportional to  $1/N^2$ .

## Acknowledgments

The authors are grateful to Prof. Luis Martínez Alonso for useful discussions.

## A Adapted SR expansions

In this Appendix we show the specific choices of  $F(\Phi)$  as well as the first few terms of the expansions for  $H(\Phi)$  for the families of potentials mentioned in the Introduction. In terms of reduced variables, eqs. (1.13), (1.14) and (1.15) read,

$$\mathfrak{h}(\varphi) = \frac{h(\varphi)}{\sqrt{v(\varphi)}}, \quad (\text{A.1})$$

$$\mathfrak{h}'(\varphi) = \sqrt{\mathfrak{h}(\varphi)^2 - 1} - \mathfrak{v}(\varphi)\mathfrak{h}(\varphi), \quad (\text{A.2})$$

$$\mathfrak{v}(\varphi) = \frac{v'(\varphi)}{2v(\varphi)}, \quad (\text{A.3})$$

respectively, with

$$\mathfrak{h}(\varphi) = \mathcal{H}(\Phi), \quad (\text{A.4})$$

$$\mathfrak{v}(\varphi) = M_{\text{Pl}} \sqrt{\frac{2}{3}} \mathcal{V}(\Phi). \quad (\text{A.5})$$

Model	$v(\varphi)$	$\mathfrak{h}(\varphi) = \frac{h(\varphi)}{\sqrt{v(\varphi)}}$
MLFI	$A\varphi^2 (a\varphi^2 + 1)$	$1 + \frac{2}{\varphi^2} - \frac{2(a+1)}{a\varphi^4} + \frac{24a^2+16a+5}{2a^2\varphi^6} - \dots$
DWI	$A (a\varphi^2 - 1)^2$	$1 + \frac{2}{\varphi^2} - \frac{2(a-2)}{a\varphi^4} + \frac{2(6a^2-8a+3)}{a^2\varphi^6} - \dots$
GMSSMI	$A (\varphi^2 - a\varphi^6 + b\varphi^{10})$	$1 + \frac{25}{2\varphi^2} + \frac{875}{8\varphi^4} + \frac{5(32a-375b)}{16b\varphi^6} + \dots$
GRIPI	$A (\varphi^2 - a\varphi^3 + b\varphi^4)$	$1 + \frac{2}{\varphi^2} + \frac{a}{b\varphi^3} + \frac{9a^2-16b^2-16b}{8b^2\varphi^4} + \dots$
SSBI	$A (1 + a\varphi^2 + b\varphi^4)$	$1 + \frac{2}{\varphi^2} - \frac{2(a+b)}{b\varphi^4} + \frac{5a^2+16ab+24b^2-8b}{2b^2\varphi^6} + \dots$
HFII	$A(a\varphi + 1)^2 \left(1 - \frac{a^2}{(a\varphi+1)^2}\right)$	$1 + \frac{1}{2\varphi^2} - \frac{1}{a\varphi^3} + \frac{3(a^4+4)}{8a^2\varphi^4} + \dots$
RGI	$\frac{A\varphi^2}{a+\varphi^2}$	$1 + \frac{a^2}{2\varphi^6} - \frac{a^3}{\varphi^8} + \frac{3(a^4-2a^3)}{2\varphi^{10}} + \dots$
CSI	$\frac{A}{(1-a\varphi)^2}$	$1 + \frac{1}{2\varphi^2} + \frac{1}{a\varphi^3} + \frac{11a^2+12}{8a^2\varphi^4} + \dots$
LFI	$A\varphi^p$	$1 + \frac{p^2}{8\varphi^2} + \frac{p^3(3p-16)}{128\varphi^4} + \frac{p^4(5p^2-80p+288)}{1024\varphi^6} + \dots$
IMI	$A\varphi^{-p}$	$1 + \frac{p^2}{8\varphi^2} + \frac{p^3(3p+16)}{128\varphi^4} + \frac{p^4(5p^2+80p+288)}{1024\varphi^6} + \dots$

**Table 4.** First four terms of the expansions for the Hubble parameter  $\mathfrak{h}(\varphi)$  as inverse power series in  $f(\varphi) = \varphi$  for polynomial, rational and monomial potentials with non-integer exponent  $p$  taken from Ref. [7]. The relation between the parameters  $A$ ,  $a$  and  $b$  in this table and the physical parameters in Ref. [7] is given in Table 5.

If  $\mathfrak{v}(\varphi)$  is of the form

$$\mathfrak{v}(\varphi) = Q(f(\varphi)), \quad (\text{A.6})$$

where  $f(\varphi) \rightarrow \infty$  as  $\varphi \rightarrow \infty$ , and  $Q$  has a suitable Taylor expansion as  $f(\varphi) \rightarrow \infty$ , then eq. (A.2) has a formal solution in inverse powers of  $f(\varphi)$ .

For example, if the potential  $v(\varphi)$  is a rational function of  $\varphi$  (and in particular, a polynomial function), so is  $\mathfrak{v}(\varphi)$ , and therefore the choice

$$f(\varphi) = \varphi, \quad (\text{A.7})$$

is suitable for all these potentials. The same choice works for monomial potentials with non-integer exponents, because again  $\mathfrak{v}(\varphi)$  is a rational function of  $\varphi$  (more concretely, proportional to  $1/\varphi$ ). In Table 4 we list the first four terms of the expansions of  $\mathfrak{h}(\varphi)$  for some polynomial, rational and for two monomial potentials with non-integer exponents  $p$  taken from Ref. [7], and in Table 5 we give the relation between the parameters  $A$ ,  $a$  and  $b$  in Table 4 and the corresponding physical parameters in Ref. [7]. We have not included in the table particular instances of these polynomial potentials: For example, MSSMI is the particular case of GMSSMI with  $b = 9a^2/20$ , and RIPI is the particular case of GRIPI with  $b = 9a^2/32$ .

Our second set of examples pertains to potentials wherein the inflaton appears either as a rational function of an exponential or even as the exponential of a rational function of an exponential, and comprises potentials taken from Ref. [7] and  $\alpha$ -attractors taken from Refs. [2] and [16]. In all these cases  $\mathfrak{h}(\varphi)$  can be systematically expanded as a formal series in inverse powers of

$$f(\varphi) = e^{\lambda\varphi}, \quad (\text{A.8})$$

Model	$A$	$a$	$b$
MLFI	$\frac{2M^4}{M_{\text{Pl}}^2}$	$\frac{2}{3}\alpha$	
DWI	$\frac{3M^4}{M_{\text{Pl}}^2}$	$\frac{2M_{\text{Pl}}^2}{3\phi_0^2}$	
GMSSMI	$\frac{2M^4}{\phi_0^2}$	$\frac{8M_{\text{Pl}}^4}{27\phi_0^4}\alpha$	$\frac{16M_{\text{Pl}}^8}{405\phi_0^8}\alpha$
GRIFI	$\frac{2M^4}{\phi_0^2}$	$\frac{4\sqrt{2}M_{\text{Pl}}}{3\sqrt{3}\phi_0}\alpha$	$\frac{M_{\text{Pl}}^2}{3\phi_0^2}\alpha$
SSBI	$\frac{3M^4}{M_{\text{Pl}}^2}$	$\frac{2}{3}\alpha$	$\frac{4}{9}\beta$
HF1I	$\frac{3M^4}{M_{\text{Pl}}^2}$	$\sqrt{\frac{2}{3}}A_1$	
RGI	$\frac{3M^4}{M_{\text{Pl}}^2}$	$\frac{3}{2}\alpha$	
CSI	$\frac{3M^4}{M_{\text{Pl}}^2}$	$\sqrt{\frac{2}{3}}\alpha$	
LFI	$\left(\frac{2}{3}\right)^{\frac{p}{2}}\frac{3M^4}{M_{\text{Pl}}^2}$		
IMI	$\left(\frac{2}{3}\right)^{-\frac{p}{2}}\frac{3M^4}{M_{\text{Pl}}^2}$		

**Table 5.** Relation between the parameters  $A$ ,  $a$  and  $b$  in Table 4 and the physical parameters in Ref. [7].

in some cases for a particular, fixed value of  $\lambda$ . Table 6 shows the first three terms of these expansions and Table 7 shows the relations between the parameters  $A$  and  $\lambda$  in Table 6 and the physical parameters in Refs. [2, 7, 16].

An additional simplification occurs if the potential  $v(\varphi)$  is an even function of  $f(\varphi)$ , wherein odd powers of  $1/f(\varphi)$  do not appear in the expansions and we can expand directly in  $1/f(\varphi)^2$ .

The key point exemplified in Tables 4 and 6 is that by using a suitable  $f(\varphi)$  adapted to each (family of) potential(s), a systematic rearrangement of the SR expansion as a formal series in inverse powers of  $f(\varphi)$  can be efficiently computed to any desired order, which in turn allows us the consistent use of summation methods as discussed in the following Appendix.

## B Padé approximants

Partial sums of divergent asymptotic expansions (e.g., those obtained from perturbation theory) usually yield very limited accuracy even when used over narrow ranges of the independent variable. To overcome this limitation, and dating back to work in the 1970's on the perturbation theory of the quartic anharmonic oscillator [45], the use of rational approximants and in particular of Padé approximants [31] derived from the formal power series has proved useful in a variety of fields. Although in some important cases it has been proved that Padé approximants of increasing order ultimately converge to the exact solution of the problem [45], Padé approximants are typically used on an empirical basis, which is the approach we take here to sum both the SR and the KD series. For completeness, we illustrate the method in the case of the SR series (3.10),

$$\hat{h}_{\text{SR}}(y) = \sqrt{A} \left( \frac{1-y}{1+y} \right)^m \tilde{h}_{\text{SR}}(y), \quad (\text{B.1})$$

Model	$v(\varphi)$	$h(\varphi) = \frac{h(\varphi)}{\sqrt{v(\varphi)}}$
HI	$A \left( 1 - e^{-\frac{2\varphi}{3}} \right)$	$1 + \frac{2}{9}e^{-\frac{4\varphi}{3}} + \frac{20}{81}e^{-2\varphi} + \dots$
ESI	$A \left( 1 - e^{-\lambda\varphi} \right)$	$1 + \frac{1}{8}\lambda^2 e^{-2\lambda\varphi} + \frac{1}{8} \left( 2\lambda^2 - \lambda^4 \right) e^{-3\lambda\varphi} + \dots$
MHI	$A \left( 1 - \operatorname{sech}(\lambda\varphi) \right)$	$1 + \frac{\lambda^2}{2} e^{-2\lambda\varphi} + \left( 2\lambda^2 - \lambda^4 \right) e^{-3\lambda\varphi} + \dots$
CNAI	$A \left( 1 - \left( 1 + \lambda^2 \right) \tanh^2(\lambda\varphi) \right)$	$1 + \frac{8(1+\lambda^2)^2}{\lambda^2} e^{-4\lambda\varphi} - \frac{64(2\lambda^8+6\lambda^6+5\lambda^4-1)}{\lambda^4} e^{-6\lambda\varphi} + \dots$
CNCI	$A \left( \left( 1 + \lambda^2 \right) \coth^2(\lambda\varphi) - 1 \right)$	$1 + \frac{8(1+\lambda^2)^2}{\lambda^2} e^{-4\lambda\varphi} + \frac{64(2\lambda^8+6\lambda^6+5\lambda^4-1)}{\lambda^4} e^{-6\lambda\varphi} + \dots$
T	$A \left( \tanh^2(\lambda\varphi) \right)^n$	$1 + 8n^2 \lambda^2 e^{-4\lambda\varphi} - 128n^3 \lambda^4 e^{-6\lambda\varphi} + \dots$
E	$A \left( 1 - e^{-2\lambda\varphi} \right)^{2n}$	$1 + 2n^2 \lambda^2 e^{-4\lambda\varphi} - 4n^2 \lambda^2 \left( 4n\lambda^2 - 1 \right) e^{-6\lambda\varphi} + \dots$
Linear	$A \left( \tanh(\lambda\varphi) + 1 \right) + B$	$1 + \frac{2A^2\lambda^2}{(2A+B)^2} e^{-4\lambda\varphi} - \frac{8A^2\lambda^2(A(2\lambda^2+1)+B)}{(2A+B)^3} e^{-6\lambda\varphi} + \dots$
Two-shoulder	$A \left( \exp(\gamma \tanh(\lambda\varphi)) - 1 \right)^2$	$1 + \frac{8\gamma^2\lambda^2 e^{2\gamma}}{(e^\gamma-1)^2} e^{-4\lambda\varphi} - \frac{32\gamma^2\lambda^2(e^\gamma(4\gamma\lambda^2+1)-\gamma-1)e^{2\gamma}}{(e^\gamma-1)^3} e^{-6\lambda\varphi} + \dots$
Exp-I	$A \exp(\gamma \tanh(\lambda\varphi))$	$1 + 2\gamma^2 \lambda^2 e^{-4\lambda\varphi} - 8\gamma^2 \lambda^2 \left( 1 + 2\gamma\lambda^2 \right) e^{-6\lambda\varphi} + \dots$
Exp-II	$A \left( \exp(\gamma \tanh(\lambda\varphi) + 1) \right) - 1$	$1 + \frac{2\gamma^2\lambda^2 e^{4\gamma}}{(e^{2\gamma}-1)^2} e^{-4\lambda\varphi} - \frac{8\gamma^2\lambda^2 e^{4\gamma}(e^{2\gamma}(1+2\gamma\lambda^2)-\gamma-1)}{(e^{2\gamma}-1)^3} e^{-6\lambda\varphi} + \dots$

**Table 6.** First three terms of the expansions for the Hubble parameter  $h(\varphi)$  as inverse power series in  $f(\varphi) = e^{\lambda\varphi}$  for some potentials taken from Ref. [7] and for  $\alpha$ -attractors taken from Refs. [2] and [16]. In the linear model it is assumed that  $B \ll A$ . The relation between the parameters  $A$  and  $\lambda$  in this table and the physical parameters in Ref. [7] is given in Table 7, and the relation of the parameter  $B$  in the caption of Table 7.

Model	$A$	$\lambda$
HI	$\frac{3M^4}{M_{\text{Pl}}^2}$	
ESI	$\frac{3M^4}{M_{\text{Pl}}^2}$	$\sqrt{\frac{2}{3}}q$
MHI	$\frac{3M^4}{M_{\text{Pl}}^2}$	$\sqrt{\frac{2}{3}}\frac{M_{\text{Pl}}^2}{\mu}$
CNAI and CNCI	$\frac{9M^4}{M_{\text{Pl}}^2}$	$\frac{\alpha}{\sqrt{3}}$
T and E	$3\alpha\mu^2$	$\frac{1}{3\sqrt{\alpha}}$
Linear	$3\gamma\sqrt{6\alpha}$	$\frac{1}{3\sqrt{\alpha}}$
Exp-I	$3M^2e^{-\gamma}$	$\frac{1}{3\sqrt{\alpha}}$
Two-shoulder and Exp-II	$3M^2e^{-2\gamma}$	$\frac{1}{3\sqrt{\alpha}}$

**Table 7.** Relation between the parameters  $A$  and  $\lambda$  in Table 6 and the physical parameters in Refs. [2, 7, 16]. In the Linear model,  $B = 3\Lambda$

where we have denoted with a tilde the formal power series in  $y$ ,

$$\tilde{h}_{\text{SR}}(y) = 1 + 8m^2\lambda^2 \sum_{n=2}^{\infty} (-1)^n c_n y^n. \quad (\text{B.2})$$

Instead of using a partial sum,

$$\tilde{h}_{\text{SR}}^{[n_{\text{SR}}]}(y) = 1 + 8m^2\lambda^2 \sum_{n=2}^{n_{\text{SR}}} (-1)^n c_n y^n, \quad (\text{B.3})$$

which yields very limited accuracy and ultimately diverges, we use the  $[n_{\text{SR}}/n_{\text{SR}} + 1]$  Padé approximant, which is defined as the rational function with numerator of degree  $n_{\text{SR}}$  and denominator of degree  $n_{\text{SR}}+1$  whose Taylor series as  $y \rightarrow 0$  has the same  $2n_{\text{SR}}+1$  coefficients as the given series  $\tilde{h}_{\text{SR}}$ , i.e., the rational function

$$\tilde{h}_{\text{SR}}^{[n_{\text{SR}}/n_{\text{SR}}+1]}(y) = \frac{1 + 8m^2\lambda^2 \sum_{j=1}^{n_{\text{SR}}} (-1)^j \mu_j y^j}{1 + 8m^2\lambda^2 \sum_{j=1}^{n_{\text{SR}}+1} (-1)^j \nu_j y^j}, \quad (\text{B.4})$$

whose coefficients  $\mu_j$ ,  $j = 1, \dots, n_{\text{SR}}$ ,  $\nu_j$ ,  $j = 1, \dots, n_{\text{SR}} + 1$  are such that

$$\tilde{h}_{\text{SR}}^{[n_{\text{SR}}/n_{\text{SR}}+1]}(y) - \tilde{h}_{\text{SR}}^{[2n_{\text{SR}}+1]}(y) = O(y^{2n_{\text{SR}}+2}) \quad \text{as } y \rightarrow 0. \quad (\text{B.5})$$

By substituting eq. (B.3) with  $n_{\text{SR}}$  replaced by  $2n_{\text{SR}} + 1$  and eq. (B.4) into eq. (B.5) we find,

$$\begin{aligned} & \left( 1 + 8m^2\lambda^2 \sum_{n=2}^{2n_{\text{SR}}+1} (-1)^n c_n y^n \right) \left( 1 + 8m^2\lambda^2 \sum_{j=1}^{n_{\text{SR}}+1} (-1)^j \nu_j y^j \right) \\ & - \left( 1 + 8m^2\lambda^2 \sum_{j=1}^{n_{\text{SR}}} (-1)^j \mu_j y^j \right) = O(y^{2n_{\text{SR}}+2}) \quad \text{as } y \rightarrow 0. \end{aligned} \quad (\text{B.6})$$

Equating to zero the coefficients of  $y^j$ ,  $j = 1, \dots, n_{\text{SR}}$  in the left-hand side of eq (B.6) we find that, with  $c_1 = 0$ ,

$$\mu_j = \nu_j + c_j + 8m^2\lambda^2 \sum_{k=1}^{j-2} c_{j-k}\nu_k, \quad j = 1, \dots, n_{\text{SR}}, \quad (\text{B.7})$$

while equating to zero the coefficients of  $y^j$ ,  $j = n_{\text{SR}} + 1, \dots, 2n_{\text{SR}} + 1$  we find that the coefficients  $\nu_j$ ,  $j = 1, \dots, n_{\text{SR}} + 1$  are the solutions of the linear system,

$$\begin{bmatrix} 8m^2\lambda^2 c_{n_{\text{SR}}} & 8m^2\lambda^2 c_{n_{\text{SR}}-1} & \cdots & 8m^2\lambda^2 c_1 & 1 \\ 8m^2\lambda^2 c_{n_{\text{SR}}+1} & 8m^2\lambda^2 c_{n_{\text{SR}}} & \cdots & 8m^2\lambda^2 c_2 & 8m^2\lambda^2 c_1 \\ \vdots & \vdots & & \ddots & \vdots \\ 8m^2\lambda^2 c_{2n_{\text{SR}}} & 8m^2\lambda^2 c_{2n_{\text{SR}}-1} & \cdots & 8m^2\lambda^2 c_{n_{\text{SR}}+1} & 8m^2\lambda^2 c_{n_{\text{SR}}} \end{bmatrix} \begin{bmatrix} \nu_1 \\ \nu_2 \\ \vdots \\ \nu_{n_{\text{SR}}+1} \end{bmatrix} = \begin{bmatrix} -c_{n_{\text{SR}}+1} \\ -c_{n_{\text{SR}}+2} \\ \vdots \\ -c_{2n_{\text{SR}}+1} \end{bmatrix}. \quad (\text{B.8})$$

For example, for  $n_{\text{SR}} = 1$  we find that  $\mu_1 = \nu_1 = -\frac{2}{m}$ ,  $\nu_2 = -1$  and therefore

$$\tilde{h}_{\text{SR}}^{[1/2]}(y) = \frac{1 + 16m\lambda^2 y}{1 + 16m\lambda^2 y - 8m^2\lambda^2 y^2}. \quad (\text{B.9})$$

The choice of  $n_{\text{SR}}$  and  $n_{\text{SR}} + 1$  as degrees of the polynomials in the numerator and in the denominator of the approximant (B.4) is not critical (in most cases, any para-diagonal sequence of approximants can be used), and has been chosen for efficiency in the recursive solution of the system (B.8). The accuracy of this approximants as compared with numerical solutions of the corresponding equations is discussed in the main body of the paper.

## References

- [1] R. Kallosh, A. Linde and D. Roest, *Superconformal inflationary  $\alpha$ -attractors*, *J. High Energy Phys.* **2013** (2013) 1.
- [2] Y. Akrami, R. Kallosh, A. Linde and V. Vardanyan, *Dark energy,  $\alpha$ -attractors, and large-scale structure surveys*, *J. Cosmol. Astropart. Phys.* **2018** (2018) 041.
- [3] D. Chowdhury, J. Martin, C. Ringeval and V. Vennin, *Assessing the scientific status of inflation after Planck*, *Phys. Rev. D* **100** (2019) 083537.
- [4] D. Sloan, K. Dimopoulos and S. Karamitsos, *T-model inflation and bouncing cosmology*, *Phys. Rev. D* **101** (2020) 043521.
- [5] A.R. Liddle, P. Parsons and J.D. Barrow, *Formalizing the slow-roll approximation in inflation*, *Phys. Rev. D* **50** (1994) 7222.
- [6] S.L. Leach, A.R. Liddle, J. Martin and D.J. Schwarz, *Cosmological parameter estimation and the inflationary cosmology*, *Phys. Rev. D* **66** (2002) 023515.
- [7] J. Martin, C. Ringeval and V. Vennin, *Encyclopaedia inflationaris*, *Phys. Dark Univ.* **5–6** (2014) 75.
- [8] N. Aghanim *et al.* (Planck Collaboration), “Planck 2018 results. VI. Cosmological parameters.” arXiv:1807.06209.

- [9] Y. Akrami *et al.* (Planck Collaboration), “Planck 2018 results. X. Constraints on inflation.” arXiv:1807.06211.
- [10] M. Galante, R. Kallosh, A. Linde and D. Roest, *Unity of Cosmological Inflation Attractors*, *Phys. Rev. Lett.* **114** (2015) 141302.
- [11] R. Kallosh and A. Linde, *Planck, LHC, and  $\alpha$ -attractors*, *Phys. Rev. D* **91** (2015) 083528.
- [12] D. Salopek and J. Bond, *Nonlinear evolution of long-wavelength metric fluctuations in inflationary models*, *Phys. Rev. D* **42** (1990) 3936.
- [13] S. Ferrara, R. Kallosh, A. Linde and M. Porrati, *Minimal supergravity models of inflation*, *Phys. Rev. D* **88** (2013) 085038.
- [14] S. Ferrara, P. Fre and A.S. Sorin, *On the topology of the inflaton field in minimal supergravity models*, *J. High Energy Phys.* **04** (2014) 095.
- [15] R. Kallosh, A. Linde and D. Roest, *Large field inflation and double  $\alpha$ -attractors*, *J. High Energy Phys.* **08** (2014) 052.
- [16] J.J.M. Carrasco, R. Kallosh and A. Linde, *Cosmological attractors and initial conditions for inflation*, *Phys. Rev. D* **92** (2015) 063519.
- [17] G. Germán, *On the  $\alpha$ -attractor T-models*, *J. Cosmol. Astropart. Phys.* **09** (2021) 017.
- [18] G. Álvarez, L. Martínez Alonso, E. Medina and J.L. Vázquez, *Separatrices in the Hamilton–Jacobi formalism of inflaton models*, *J. Math. Phys.* **61** (2020) 043501.
- [19] W. Handley, S. Brechet, A. Lasenby and M.P. Hobson, *Kinetic initial conditions for inflation*, *Phys. Rev. D* **89** (2014) 063505.
- [20] W. Handley, A. Lasenby and M. Hobson, *Kinetically dominated curved universes: Logolinear series expansions*, *Phys. Rev. D* **99** (2019) 123512.
- [21] L. Hergt, W. Handley, M. Hobson and A. Lasenby, *Constraining the kinetically dominated universe*, *Physical Review D* **100** (2019) 023501.
- [22] V.A. Belinskii, L.P. Grishchuk, Y.B. Zel’dovich and I.M. Khalatnikov, *Inflationary stages in cosmological models with a scalar field*, *Phys. Lett. B* **155** (1985) 232.
- [23] E.J. Copeland, A.R. Liddle and D. Wands, *Exponential potentials and cosmological scaling solutions*, *Phys. Rev. D* **57** (1998) 4686.
- [24] N. Tamanini, *Dynamics of cosmological scalar fields*, *Phys. Rev. D* **89** (2014) 083521.
- [25] A. Paliathanasis, M. Tsamparlis, S. Basilakos and J.D. Barrow, *Dynamical analysis in scalar field cosmology*, *Phys. Rev. D* **91** (2015) 123535.
- [26] A. Alho and C. Uggla, *Global dynamics and inflationary center manifold and slow-roll approximants*, *J. Math. Phys.* **56** (2015) 012502.
- [27] A. Alho and C. Uggla, *Scalar field deformations of  $\Lambda$ CDM cosmology*, *Phys. Rev. D* **92** (2015) 103502.
- [28] A. Alho and C. Uggla, *Inflationary  $\alpha$ -attractor cosmology: A global dynamical systems perspective*, *Phys. Rev. D* **95** (2017) 083517.
- [29] E. Medina and L. Martínez Alonso, *Kinetic dominance and psi series in the Hamilton–Jacobi formulation of inflaton models*, *Phys. Rev. D* **102** (2020) 103517.

- [30] E. Medina and L. Martínez Alonso, *Asymptotic solutions of a generalized Starobinski model: Kinetic dominance, slow roll and separatrices*, *Universe* **7** (2021) 500.
- [31] G.A. Baker and P. Graves-Morris, *Padé Approximants*, Cambridge University Press (1996).
- [32] R. Kallosh and A. Linde, *Universality class in conformal inflation*, *J. Cosmol. Astropart. Phys.* **2013** (2013) 002.
- [33] R. Kallosh and A. Linde, *Non-minimal inflationary attractors*, *J. Cosmol. Astropart. Phys.* **2013** (2013) 033.
- [34] R. Kallosh and A. Linde, *Escher in the sky*, *Comptes Rendus Physique* **16** (2015) 914.
- [35] Y. Akrami, S. Casas, S. Deng and V. Vardanyan, *Quintessential  $\alpha$ -attractor inflation: forecasts for Stage IV galaxy surveys*, *J. Cosmol. Astropart. Phys.* **2021** (2021) 006.
- [36] S.D. Odintsov and V.K. Oikonomou, *Inflationary  $\alpha$ -attractors from  $F(R)$  gravity*, *Phys. Rev. D* **94** (2016) 124026.
- [37] D. Baumann, *Tasi Lectures on Inflation*, TASI Lectures on Inflation, *preprint arXiv:0907.5424* (2009) .
- [38] D.H. Lyth and A.R. Liddle, *The Primordial Density Perturbation: Cosmology, Inflation and the Origin of Structure*, Cambridge University Press (2009).
- [39] D.S. Goldwirth and T. Piran, *Initial conditions for inflation*, *Phys. Rep.* **214** (1992) 223.
- [40] G. Álvarez, L. Martínez Alonso and E. Medina, *Kinetic dominance and the wave function of the Universe*, *Phys. Rev. D* **105** (2022) 083502.
- [41] D. Baumann, *Cosmology, Part III Mathematical Tripos* (2012) .
- [42] S. Dodelson, *Modern Cosmology*, Press, New York, USA (2003) .
- [43] J. Martin, *The Theory of Inflation*, in *200th Course of Enrico Fermi School of Physics: Gravitational Waves and Cosmology*, 7, 2018 [[1807.11075](#)].
- [44] F.W.J. Olver, D.W. Lozier, R.F. Boisvert and C.W. Clark, *NIST Handbook of Mathematical Functions*, Cambridge University Press (2010).
- [45] B. Simon, *Coupling constant analyticity for the anharmonic oscillator*, *Ann. Phys.* **58** (1970) 76.